the effect of Lithium oxide terminations on the thermionic properties of boron-Nitrogen co doped diamond film

Author: Ashley Tom

April 2024

Supervisor: Neil Fox

2nd Assessor: Paul May

Field: Physical and theoretical chemistry

Word count:

This thesis is submitted in partial fulfilment of the requirements for Master of Science; Chemistry (F105)

School of Chemistry

UNIVERSITY of BRISTOL

Abstract

This project investigates the effect of lithium oxide terminations on boron and nitrogen doped diamond films. Lithium oxide terminations have been experimentally validated as a species which produces negative electron affinity (NEA) on a doped and undoped diamond surfaces. This phenomenon of NEA is desirable for the application of thermionic emitting devices, as the presence of the species allows for a mean-free path for electrons to escape a diamond surface, as well as reduce the work function necessary for the liberation of electrons.

In terms of doping, a sufficient N-type semiconductor is yet to be commonplace within the field of diamond research. The most utilised N-type dopant is nitrogen; however, nitrogen exhibits a deep donor level which gives a less than desirable fermi level for the diamond film. The addition of Co-dopant species in conjunction with nitrogen have been studied with varying results.

Growths of the diamond film utilised the microwave power assisted chemical vapour deposition setup to drive doped diamond growth using diborane and nitrogen gas as dopants. The initial 3 hours of growth was doped with boron only before it was replaced with the nitrogen carrier gas.

Observations via SEM and XPS indicated the diffusion of boron species upwards through the film, with a characteristic checkered pattern growth under SEM. Work function calculations were performed using ultraviolet photoemission spectroscopy produce spectra indicative of the electronic structure of the diamond samples. A reduction in work function was observed from the H-BNDD sample to the LiO-BNDD sample, validating the claim that lithium oxide terminations exhibit greater NEA than hydrogen.

Acknowledgements

Firstly, I'd like to thank my supervisor Professor Neil fox for the opportunity to work within the Bristol diamond lab. His assistance in planning the overall scope of the project was invaluable and for that I offer my sincerest gratitude.

I would also like to give thanks to Ramiz Zulkharnay. His assistance from the beginning of the project with regards to training on equipment, assistance in understanding the underlying theory behind diamond synthesis, and general support has made my time working on the project very enjoyable.

I would like to give appreciate Jude Laverock and Jean-Charles Eloi for their continuous assistance with performing analysis on the nanoESCA and SEM.

I'd like to thank all other members of the Bristol university diamond lab group, from my peers in working in undergrad to the PHD students, postdoctoral researchers and professors. I have thoroughly enjoyed working alongside you all.

Lastly, I'd like to dedicate my thesis to my partner amelia, for the endless emotional support she has given me this year and throughout my degree, without her I wouldn't be where I am today.

Authors declaration

I declare that the work in this dissertation was carried out in accordance with the requirements of the University's Regulations and Code of Practice for Research Degree Programmes and that it has not been submitted for any other academic award. Except where indicated by specific reference in the text, the work is the candidate's own work. Work done in collaboration with, or with the assistance of, others, is indicated as such. Any views expressed in the dissertation are those of the author.

SIGNED: .... DATE: 10/04/23 ....

Contents

1- Introduction; Diamond overview

1.1- Carbon allotropes

Carbon is an abundant element on earth and in the universe, being the 17th and 6th most populous element respectively[1]. On earth, while carbon within molecular structures can be found universally, elemental carbon is much rarer, accounting for only 0.2% of the mass of the earth's crust [2]. Carbon's mass and electron configuration makes carbon an extremely versatile element in terms of creating molecular structures. Carbon atoms hold four valent electrons in its outer shell, allowing for a range of bonding to occur. Extended carbon bonding gives rise to macromolecular structures that vary in physical properties. Most pure carbon allotropes consist of repeating units of Sp2 hybridised atoms, the most common allotrope being graphite, a material made from intermolecularly bonded layers of graphene constituents. Graphene serves as the basis for most allotropic structures consisting of sp2 carbons [3], such as carbon nanotubes, a structure commonplace in nano structural research [4]. Other allotropes take on unconventional structures such as amorphous carbon, which is a porous structure currently being researched for application in hydrogen storage [5].

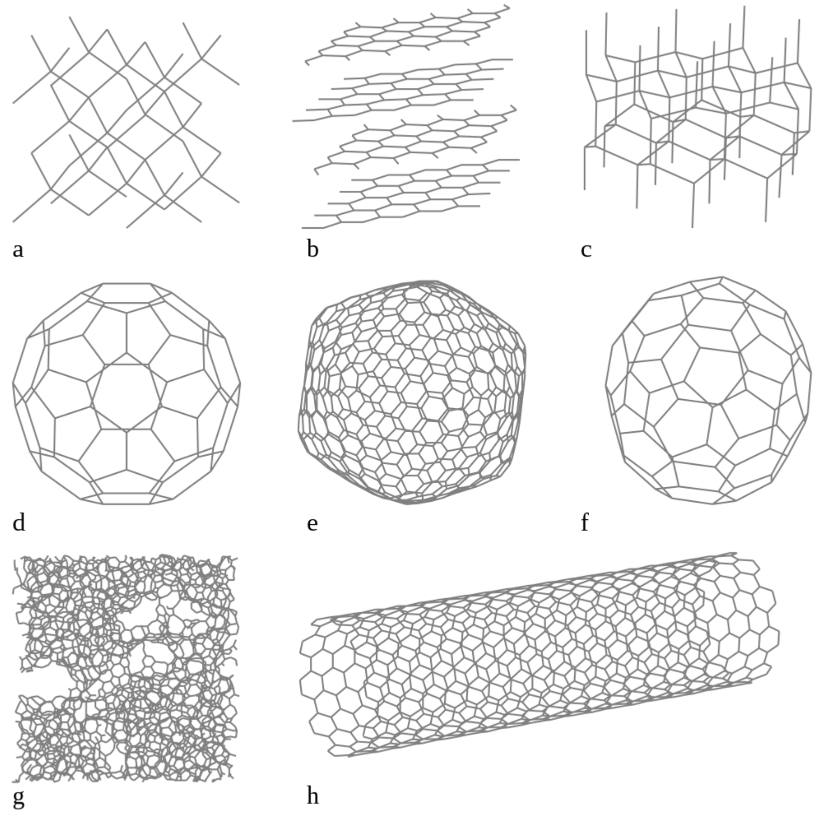

Figure 1: Carbon allotrope structures. a-c) conventional allotropes, d-f) fullerenes, g) amorphous carbon, h) carbon nanotubes[6]

Sp2 carbon allotropes form extensive pi resonant structures which readily enables the conductivity of electricity[3]. This makes such allotropes promising for a cost-effective alternative to the production of low voltage electrical devices such as sensors [7].

1.2- Natural and synthetic diamond

Naturally occurring diamond is mined in several regions across the globe. By order of quantity of diamonds mined (per carat), Russia (41,923,910), Botswana (24,752,957) and Canada (16,249,218) [8] are the countries that produce the largest quantities of diamond.

Naturally occurring diamond is resultant of high pressure and temperature conditions (>4GPa and 950-1400°) found deep within the earth's crust (>80KM) [9]. The migration of diamonds to surface level occurs via the movement of kimberlite magma from the earth's mantle to the surface via volcanic eruption. It is estimated the most recent eruption was 100 million years ago, making many of the diamonds mined today are hundreds of epochs old[10].

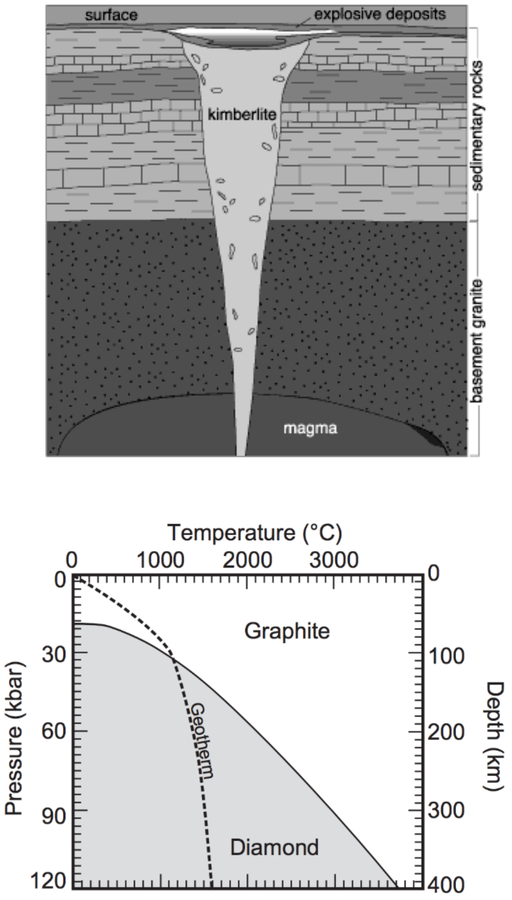

Figure 2: above) diagram of kimberlite formation in earth's crust, below) Temperature, pressure and depth profile for diamond growth[11, 12]

Despite this, it takes the movement of an average of 250 tons of earth per carat of diamond obtained, leading to a high market price for naturally occurring diamond[13-15].

Compared to natural diamond, which can vary drastically in price (between £2,000 to £7,000 per carat depending on a variety of factors) [16], synthetic diamond of similar quality can be purchased for much less (~£750), with diamond nanoparticle powder selling for as little as £24.00. We can infer that the large disparity in pricing is consequence of both the sourcing of a given diamond, as well as the application. Only a fraction of the natural diamond produced is of gem quality thus the primary application of diamond is industrial application. Though synthetic diamonds are regarded as less labour intensive, mining has a shorter time of labour per carat (0.43 hours worked per carat compared to 0.93 for HPHT lab grown diamonds).

1.3- Diamond structure

1.3.1- Bonding

Unlike other allotropes, diamond's structure consists of sp3 hybridisations, where the 2s and all 2p orbitals overlap one another forming a degenerate system where each orbital can have a strong sigma bond characteristic. This varies from sp2 systems where only 2 orbitals are sigma-pi degenerate. Consequentially, a pi orbital readily sits perpendicular to the degenerate orbitals to produce a pi-pi interaction between bonds.

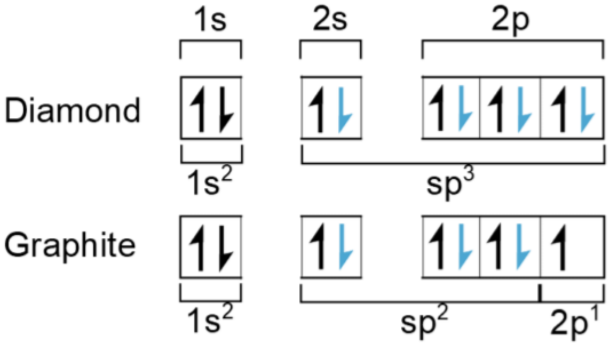

Figure 3: Diamond and graphite orbital configurations

The high sigma bonding character has greater directionality thus the overlap observed is much greater than in the sp2 structures, creating more consolidated bonding array.

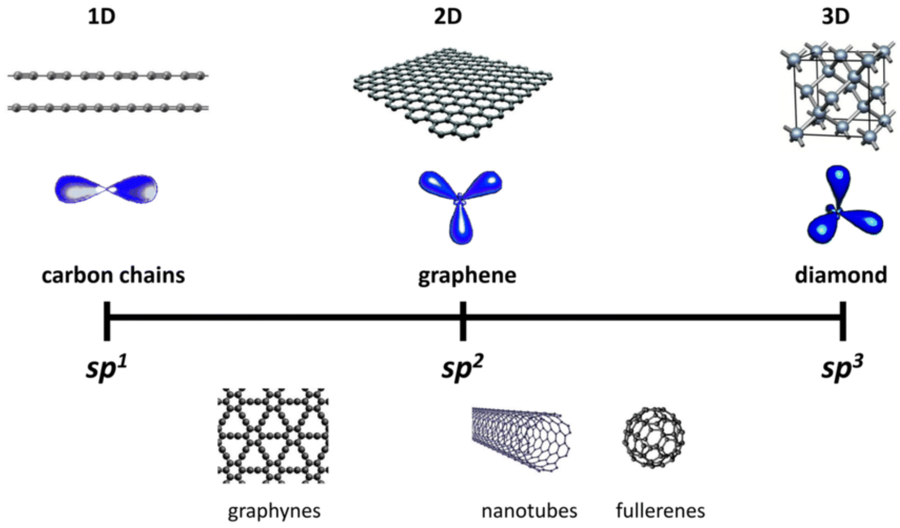

Figure 4: Carbon hybridisation and macromolecular structure scale

1.3.2- Unit cell

The diamond crystal resides in the cubic crystal family (or hexagonal in the case of Lonsdaleite), with a 3.57A unit cell length in cubic form. The diamond cubic has a *face-centred cubic* Bravais lattice structure. Due to the size of the unit cell, a single C-C bond spans only a quarter of the unit ($\frac{1}{4}, \frac{1}{4}, \frac{1}{4}$). Despite being a densely packed unit cell, the atom packing efficiency of diamond is only ~0.34 [17], which is inefficient compared to other crystal structures such as Hexagonal close-packed, with atom packing factor of 0.74[18] . In the case of metallic bonding, this lattice structure would be detrimental to the physical properties of a given material, such as in the case of tin, however, the covalent nature of diamond gives rise to a structure with extreme physical properties [001] [19].

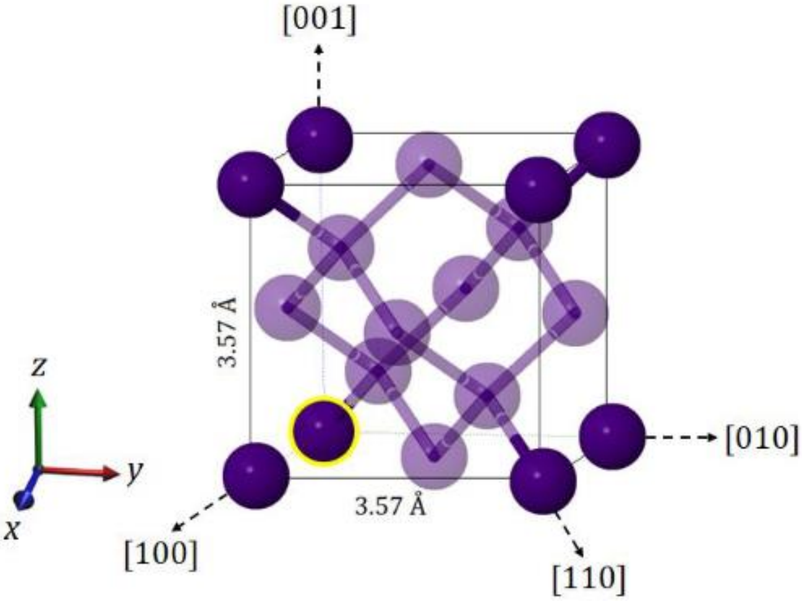

Figure 5: diamond cubic unit cell with annotated unit cell length and miller indices[19]

In terms of crystal stacking, diamonds crystal structures can be separated by their polytype. Diamond exhibits 3C and 2H polytypes for its respective crystal structures, giving rise to stacking sequences [A,B,C,A,B,C] and [A,B,A,B,A,B]. Physically, the two polymorphs can be deduced from one another by colour, as Londaeite diamond is yellow in colour. Additional polymorphs exist between these two polytypes and vary in hexagonality expressed [20].

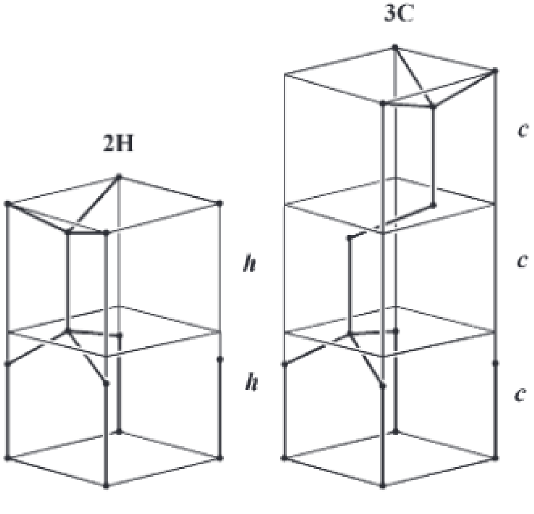

Figure 6: Stacking configurations of diamond in unit cells[20]

The difference in structure from both stacking types can be described as the 60-degree rotation of

This dense symmetric structure of covalently bonded carbons can account for many of diamonds resistant properties. Its atomic number density is calculated as 1.76 × 1029 m^{-3} or 6,556 amg. Though its mass density is calculated as 3516 kg m-3, which is validated by the experimental value for diamond (3515.25 kg m-3). This minimal difference in calculated and experimental density values can be accounted for by the inability to sequester defects in an experimental setting, negatively skewing the experimental value.

1.3.3- Symmetry

Diamond's crystal structure has a high degree of symmetry, it's Bravais character means that each carbon atom is indistinguishable from one another. In terms of diamonds space group, it Fd3m. From this annotation, we can determine that diamond has a large space group number (227) and large order number (48). [21]

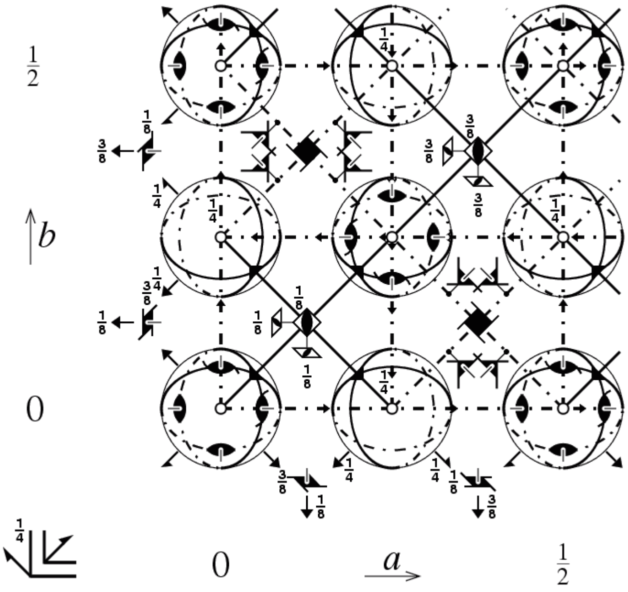

Figure 7: Depiction of the many symmetry operations performed on diamond[21]

1.3.4- Orientations

A unit cell comprised of an array of atoms can differ in structure along a given plane. In terms of crystal planes, they can be denoted by vector annotation (known as miller indices), in diagrams, we will denote the X, Y, Z axis planes by the vector [100], [010], [001] respectively. Different crystal planes exhibit different configurations of atom, the comparison of (100) and (110) being a prime example of this. It's key point to note as the surface orientation of substrates and grown diamond (specifically single crystal diamonds) can influence the measured properties of the sample (further elaboration in later sections).

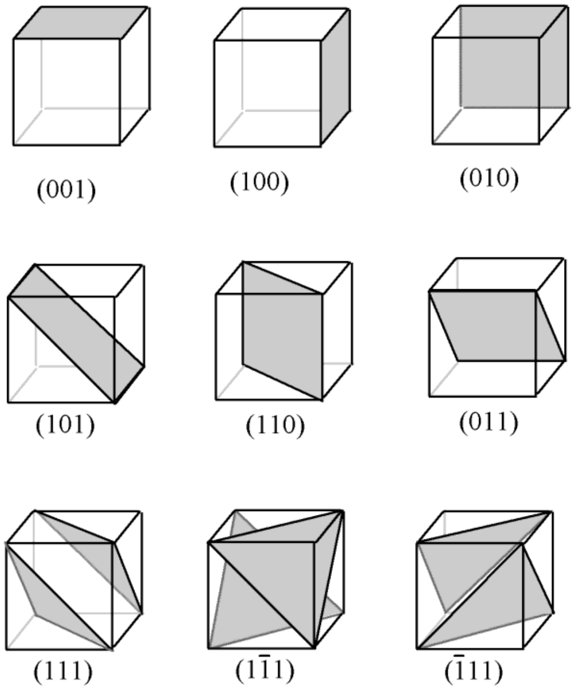

Figure 8: Miller indices planes[22]

1.4- Diamond properties

1.4.1- Physical properties & applications

Diamonds vast array of physical, chemical and electrically resistive properties, as well as its wide spectral range transparency has made diamond a popular option for applications involving extreme environments. Diamond's dense C-C bonded crystalline structure gives diamond it's characteristic hardness (4700-10,400 kgmm^{-2} a rating of 10 on the Mohs scale) [23], chemical inertness (720-800C in O_2 to degrade to CO2, melting point of 4000C). Such properties make diamond favourable for application within drilling equipment, where physical stresses and high temperatures quickly degrade conventional equipment. Furthermore, its wide spectral range transparency (1500-4000cm^{-1}) coupled with its low coefficient of expansion (1x10^{-6} K^{-1}) [24, 25] makes it desirable for applications such as watch glasses for high pressure and temperature apparatus or for use in optical equipment. Other Potential applications include the implementation of diamond film in audio equipment due to its high elastic moduli (1050Gpa) [23, 26] or heat sinks and high voltage electrical equipment due to its exceptional thermal conductivity. In recent times, diamond fabrication in diodes [27], Photo/radio-detectors[28] and thermionic devices[28] has seen persistent reported success, making future implementation more likely to be commonplace.

1.4.2- Electronic properties & applications

The primary drawback of pure diamond is its lack of conductivity. However, in the case of doped diamond, it can present with a variety of electronic characteristics with potential and real application in a variety of scenarios. For example, Boron doped diamond has seen an increased prevalence within the biomedical sector for its use within biosensors. [29] Furthermore, the focal point of current diamond research comes from the envisioned application of N-doped diamond materials that can be used to replace conventional electronic components within the semiconductor industry. [30]

1.4.3- Conductivity in diamond

In terms of describing a semiconductive material, we expand on the theory of atomic energy and molecular energy states and expand such into the context of a macromolecular structure of repeating atomic units. This gives rise to a band of energy states. The key regions of energy band structures are the valence and conduction bands, which are the cascading effect of the highest occupied molecular orbitals (HOMO) and lowest unoccupied molecular orbitals (LUMO) levels of the individual atomic quantum states.

The valence band refers to the cumulative population of electrons in the HOMO state for a given material. The most labile electrons within a materials structure indicates the energy necessary for an electron to adhere to the material, this is known as the fermi level and is dependent on the temperature of the material. At absolute zero (fermi level), the energy of this adhesion is constant.

For a wide band gap semiconductor such as diamond, once a threshold temperature is reached, electrons begin to populate some of the available energy states of the conduction band, enabling conductivity.

The probability of an electron populating a given energy state is defined by the Fermi function equation:

$$f(E) = \frac{1}{e^{(E-E_F)} + 1} \tag{1}$$

This statistical equation can be further manipulated to account for the available energy states within the conduction band to determine both the density of electrons residing in conduction band (density of states), and the number of electrons populating the conduction band at a given temperature. [31]

$$\rho(E) = \frac{8\sqrt{2}\pi m^{3/2}}{h^3}\sqrt{E}$$

(2)

$$N_{CB} = AT^{3/2}e^{-E_{gap}/2kT}$$

(3)

Due to intrinsic diamonds electron occupancy, there are no free electrons at room temperature to enable conductivity. Furthermore, this makes the distance between the valence band maxima (VBM) and conduction band minima (CBM), known as the band gap, very large (5.47eV). Thus, extensive thermal energy or short wavelength light (<UV) are needed to liberate electrons to the conduction band.

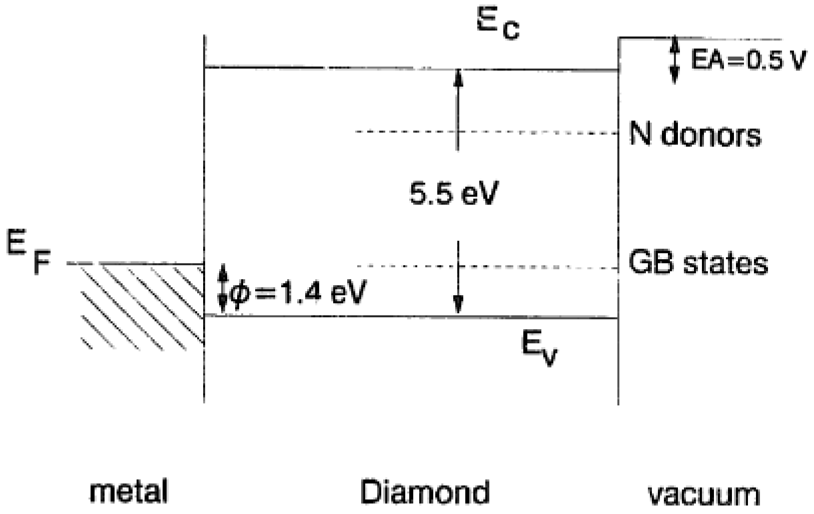

Figure 9: Band structure of bare diamond[28]

In the case of some wide band gap semiconductors, a special phenomenon can occur in materials where the vacuum level lies lower than the CBM. Electrons that's energy matches that of the vacuum is ejected from the material. This phenomenon has several implications in terms of solid-state energy research, as such the phenomenon can be used to drive electronic functionality, specifically within the application of thermionic energy convertors.

This phenomenon of negative electron affinity (NEA) can be engineered to be lower through the introduction of dopants and surface terminations, enabling the emission of electrons at lower temperatures compared to the intrinsic material. This aspect of a materials properties is the focal point of this thesis and will be explored further in later section in the context of different surface terminations and dopant species[32].

1.5- Electron emission

1.5.1- Types of emission

1.5.1.1- Nuclear decay: beta particle emission

Electron emission is the process of ejecting electrons from matter. This phenomenon is observed in the decay of radioactive atoms upon their transition down a decay chain via beta decay, where a neutron within an atom's nucleus converts to a proton, electron and electron antineutrino. An example of this is the decay of tritium:

$$ {}^{3}_{1}H \rightarrow {}^{3}_{2}He + e^{-} + \nu_{e}^{-} \tag{4} $$

This type of decay was observed by Rutherford in 1899, with the mass to charge ratio of beta particles being measured by Becquerel a year later, where he realised that the beta rays emitted from an excited nucleus of uranium was like that of J.J.Thomson's cathode rays[33, 34].

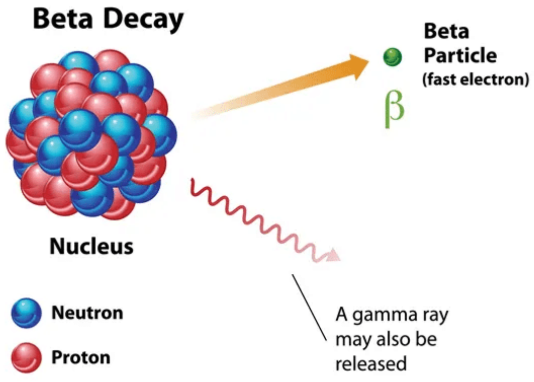

Figure 10: Beta decay from unstable nucleus[34]

The nature of radioactive species means that the emission of beta particles is dependent on decay rate of material. As radioactive nuclides are unaffected by variables such as temperature and pressure, little can be done to tune the volume of beta particles emitted from a nuclide without inducing nuclear fission. Furthermore, radioactive material decays in all directions, making it harder to capture the released beta particles efficiently.

In terms of electron emission in materials such as metals and diamond, emission of electrons occurs at the surface level via two mechanisms, thermionic emission and field electron emission[35].

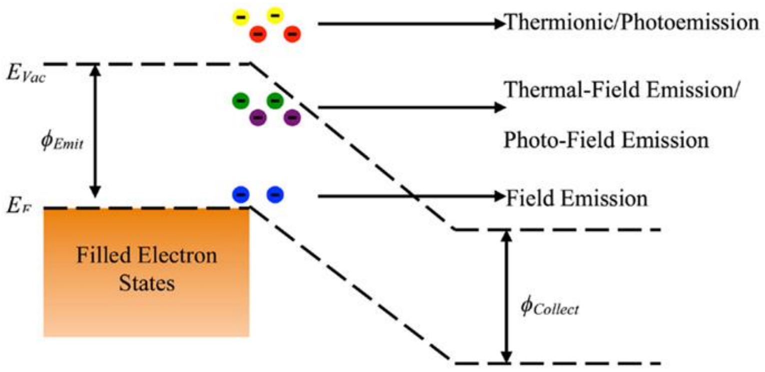

Figure 11: diagram of different pathways of electron emission[35]

1.5.1.2- Thermionic emission

Thermionic emission is defined as the liberation of electrons from a conductive surface by virtue of temperature. The energy induced by raised temperatures on a conductive surface produce sufficient energy within the surfaces band structure to emit electrons, this phenomenon is best observed in a vacuum. As temperature is the primary factor effecting the volume of electrons emitted from a surface, the current produced by a thermionic device can be tuned by the change of temperature within a certain threshold. There are two aspects governing the emission of electrons from a heated surface, the emission volume J which is proportional to temperature, and the emission threshold/ work function W. These two key parameters are further elaborated in the following sub section.

1.5.1.3- Field emission

1.5.2- Emission/temperature relationship

Field emission is the emission of electrons induced by a nearby electric field. This emission mechanism in two separate circumstances, known as Schottky emission and field electron emission.

In the case of Schottky emission (also known as field enhanced thermionic emission), the emission of electrons is induced by an electric field that is resultant of a heated thermionic surface. This effect is prominent in electron guns, where the negative bias of the emitter surface relative to its surroundings produces an electric field proportional to the volume of electrons leaving the emitter surface. Consequentially, this induced field lowers the surface barrier of the emitter, ΔW, which in turn increases the emission current. The Schottky effect is described by a modified version of the Richardson equation, and is as follows: [36, 37]

$$J\,(F,T,W) = A_G T^2 e^{-(W-\Delta W)/_{kT}}$$

(5)

$$where\ \Delta W = \sqrt{\frac{{q_e}^3 F}{4\pi\varepsilon_0}}$$

(6)

The Magnitude of the electric field F produced can be derived by the rearranging of the equation for the surface barrier threshold change ΔW, giving:

$$F = \frac{\Delta W^2\ 4\pi\varepsilon_0}{{q_e}^3}$$

(7)

The Electron field emission mechanism is akin to the Schottky effect in the sense that the field acting upon the emission surface can further drive the emission of electrons, however in this case the present field is electrostatic in nature. In the realm of applications, this electrostatic effect in most devices is undesirable due to potential vacuum breakdown and electrical discharge occurring, as well as electron drift.[38, 39]

1.5.2- Thermionic emission- History

Thermionic emission was first investigated in 1901 by Richardson where he showed how that for each unit area of a platinum[40] surface emitted a limited number of electrons when heating platinum in vacuum to a constant temperature. When further heated, the surface saw an exponential increase in the number of electrons emitted. leading him to deduce the initial equation governing the law of thermionic emission:

$$J = AT^{\frac{1}{2}} e^{-\frac{w}{kt}}$$

(8)

Where k is Boltzmann’s constant, T is the temperature of the material, W and A are constants relating to the material. The assumption Richardson gave to account for this equation was that "freely moving electrons in the interior of the hot conductor escaped when they reached the surface provided that the part of their energy which depended on the component of velocity normal to the surface was greater than the work function w". [39] Further research by Richardson determined that this hypothesis was consistent with other materials such as sodium and carbon[39]. Furthermore, He determined that the work functions for different atoms are proportional to the following parameters:

$$W \propto \frac{1}{2}(\frac{e^2}{d})$$

(9)

Where e is the electronic charge and d is the radius of the atom. These observations were further verified by Wehnelts in 1904[41] during his work with metallic oxides. However, the phenomena of electron emission were not concrete, this is due to the theory that if a hot body was in fact emitting electrons, the hot body itself should cool. Experiments performed by Wehnelts and Jentzsch in 1909 observed the cooling effect of the hot body however the magnitude of which did not agree with the proposed theory. Further experiments performed by Richardson in 1912 showed a close relationship between thermionic emission and the photoelectric effect.

$$w^0 = h\,v^0$$

(10)

Moreover, in 1913 experiments using ductile tungsten and large currents in a better vacuum than previously used showed that the total mass of electrons observed exceeded that of the total mass of electrons expected. Solidifying the theory that the emission of electrons is a physical phenomenon and not a byproduct of a reaction with any surrounding gas.[42, 43]

This evidence was further supported by Davison and Germer in 1922, confirming direct proportionality between the cooling effect and the magnitude of cooling expected in theory.

Later adjustments (with contribution from Dushman who applied quantum mechanical principles) of Equation (X) entailed, giving the thermionic emission equation known as the Richardson-Dushman equation:

$$J = AT^2 e^{(-\frac{\phi}{kT})}$$

(11)

This equation governs the density of electrons observed from an emission surface at a given temperature. [35]

1.5.3- Work function

The work function is defined as the threshold energy required to liberate electrons from the fermi level of a material to the vacuum level, where it is subsequently ejected from the surface. Whilst the relationship of atomic work function was described in the previous sub-section. For bulk materials where we distinguish its electronic structure with bands, the work function of a material is defined as the difference between the fermi level of the material and the energy of the vacuum level.

$$\phi = E_{vac} - E_F \tag{12}$$

The work function of the material is dependent on a variety of factors. The key factors being the presence of dopant species within the material and the addition of surface terminations on the diamond surface. Both can be used in conjunction to drive the reduction of work function within a diamond film. Other factors such as the field emission mechanisms stated earlier are also applicable however are of lesser focus.

1.5.3- Electron affinity at surface level

Electron affinity is described as an electrons ability to adhere to a given atomic species. In terms of thermionic emission and surface level terminations, this effect is paramount to reducing the work function. The equation for electron affinity is described as follows:

$$\chi = E_{vac} - E_{CBM} \tag{13}$$

As previously mentioned, NEA is an ideal characteristic for a diamond surface to have to drive the emission of electrons. We can infer from the above equation that to produce a surface with negative electron affinity, the vacuum level energy must be lower than that of the CBM of the bulk diamond. On the surface of diamond, the addition of species with electronegativity values of 2.6 or lower can produce a diamond surface exhibiting negative electron affinity.[44]

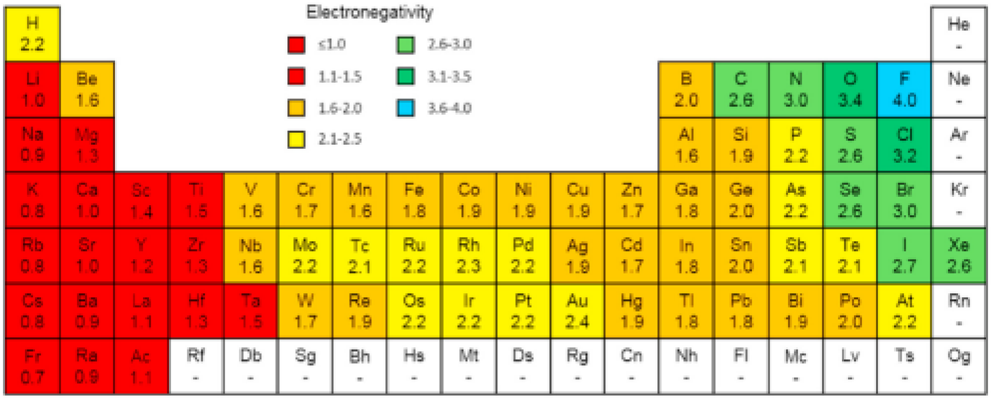

Electronegativity

🟥 ≤1.0
🟥 1.1-1.5
🟧 1.6-2.0
🟨 2.1-2.5
🟩 2.6-3.0
🟩 3.1-3.5
🟦 3.6-4.0

H 2.2																	He -
Li 1.0	Be 1.6											B 2.0	C 2.6	N 3.0	O 3.4	F 4.0	Ne -
Na 0.9	Mg 1.3											Al 1.6	Si 1.9	P 2.2	S 2.6	Cl 3.2	Ar -
K 0.8	Ca 1.0	Sc 1.4	Ti 1.5	V 1.6	Cr 1.7	Mn 1.6	Fe 1.8	Co 1.9	Ni 1.9	Cu 1.9	Zn 1.7	Ga 1.8	Ge 2.0	As 2.2	Se 2.6	Br 3.0	Kr -
Rb 0.8	Sr 1.0	Y 1.2	Zr 1.3	Nb 1.6	Mo 2.2	Tc 2.1	Ru 2.2	Rh 2.3	Pd 2.2	Ag 1.9	Cd 1.7	In 1.8	Sn 2.0	Sb 2.1	Te 2.1	I 2.7	Xe 2.6
Cs 0.8	Ba 0.9	La 1.1	Hf 1.3	Ta 1.5	W 1.7	Re 1.9	Os 2.2	Ir 2.2	Pt 2.2	Au 2.4	Hg 1.9	Tl 1.8	Pb 1.8	Bi 1.9	Po 2.0	At 2.2	Rn -
Fr 0.7	Ra 0.9	Ac 1.1	Rf -	Db -	Sg -	Bh -	Hs -	Mt -	Ds -	Rg -	Cn -	Nh -	Fl -	Mc -	Lv -	Ts -	Og -

Figure 12: periodic tabled labelled with electronegativity values[44]

When analysing the periodic table with regards to each atom's electronegativity value, we can deduce that the most alkaline and transition metal species have potential to induce NEA in a diamond film's surface. We must consider factors such as atom size of the terminating species, which for larger atoms may produce lattice mismatch between the surface boundaries. Several species have used as surface terminations both *ab initio* and experimentally, a list of terminations will be mentioned and elaborated on in later sections.

Surface terminations, coupled with dopant species within the bulk lattice, can have great effects on the band structure of a diamond material. Surface level terminations can cause band bending near the surface of the material, creating a path of "lesser resistance" for electrons to be promoted to CBM or vacuum level. In terms of species for NEA, they induce downwards band bending, reducing band gap size and subsequently produce a band structure indicating either true NEA, or effective NEA; where the vacuum level is completely beneath of the CBM and where only the band bended CBM is lesser than the vacuum level respectively. In either case, electrons circumventing the CBM of the bulk diamond lattice is desirable as it provides a mean-free pathway to electron emission.

1.5.4- Thermionic energy convertors & potential applications

Thermionic devices use the phenomena of thermionic emission to produce electrical energy. A thermionic device consists of an anode and cathode in a vacuum tube, separated by a micron scale gap. The cathode is electron source, which in conventional thermionic devices, is a metal heated to the point where electrons are liberated from the surface. The anode, another conductive surface, is impacted by the electrons ejected from the cathode. This intake of energetic electrons mobilises electrons within the anode's structure, which when both sides are connected, produces a current. This phenomenon is known as the Edison effect, after patent holder Thomas Edison (1883), and serves as the basis for thermionic energy converters (TEC).

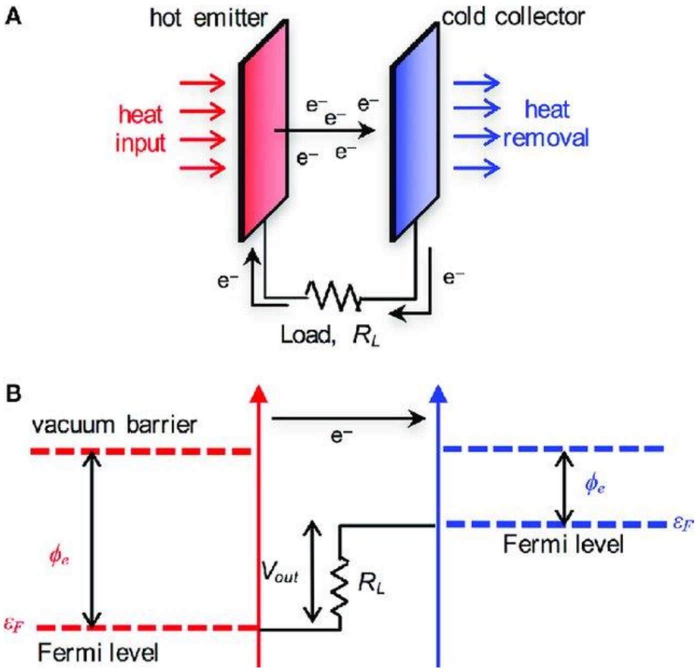

Figure 13: a) Thermionic energy converter setup, b) setup in terms of work function at collector and emitter[45]

For the effective energy transfer of electrons from the emitter to collector, it is vital that the work function for collector surface must be at least 1eV less than the emitting surface to maximise the efficiency of electron transmission. The resultant power density of the device is determined by the difference in work between electrodes and the temperature of the emitter:

$$P(T) = A_R T_E^2 e^{\left(-\phi_E/kT_e\right)}(\phi_E - \phi_C) \tag{14}$$

Where other thermal conversion methods such as thermophotovoltaic devices, which use a semiconductive material between the electrodes or a photovoltaic cell to collect the thermal energy emitted, the use of a small vacuum gap in TEC’s removes two efficiency reducing effects of conventional heat engines: the vacuum gap prevents excessive parasitic heat loss, meaning operating temperatures can exceed other devices by a wide margin.[46]

Secondly, this direct delivery of electrons from the emitter to collector means that TEC’s have the capability of being very dense in terms of power output compared to alternatives. Feasible remedies to this limitation are either to reduce the distance between the electrode to several microns, the addition of positive ions to the surface of the emitter. [38]

Modern applications for thermionic energy converters situate around the implementation of radioactive sources to drive to drive the operation of the device. Fissionable radioactive material such as plutonium-238 is energy dense and produce a very high energy decay. The radio emission of the isotope can produce heat/light for an absorber surface behind the emitter, driving the function of the TEC. Many fissionable radioactive species have very long half-lives making them suitable for devices where long-term operation is necessary, such as in batteries for space exploration devices.[47]

1.5.5- Carnot efficiency

We use the Carnot efficiency theorem to determine the maximum power output possible for a given traditional heat engine that converts heat to work. Physicist Sadi Carnot theorised that the any device that converts heat to work is comprised of two thermal reservoirs (hot and cold). As thermal energy transfers towards the cold reservoir, work is done on the system in between. In terms of TEC's, the vacuum gap employed in between the hot and cold reservoir prevents any loss of energy produced from the emission, and as the cold collector is our output electrical, the theoretical efficiency of the device is much larger than conventional heat engines.

The Carnot efficiency equation is described as follows:

$$\eta_{Carnot} = \frac{T_E}{T_E - T_C}$$

(15)

Where TE and TC is the temperature of the emitter and collector respectively. This equation can be expanded to encapsulate the differences in a TEC more accurately in the individual components as such: [44, 48]

$$\eta = \frac{J_E(V_E - V_C - V_W)}{R + H + J_E(V_E + 2kT_E)}$$

(16)

Where J_E is the current density from the emitter, $(V_E - V_C)$ is the potential difference in voltage emitter and collector surfaces. V_W is the loss of voltage from the load wire connected. R and H is the loss of heat via black-body radiation and thermal conductivity from the emitter respectively.

1.5.6- Limitations of TEC's

The most prominent energy barrier for such devices is the occurrence of the space charge effect, whereby electrons travelling in the vacuum gap repel one another as they travel across. Consequentially, this disrupts the electric current and limits the current density observed in current TEC’s. This effect in parallel planar diodes can be described by the Child-Langmuir law:[49]

$$J = \frac{I}{S} = \frac{4\varepsilon_0}{9}\sqrt{\frac{2e}{m_e}}\frac{V^{3/2}}{d^2} \tag{17}$$

Immediately, we can determine that a potential remedy to reduce this effect is by reducing the distance between the electrodes, as $J \propto 1/d^2$. This must be balanced with the potential heat transfer between electrodes, however, as a shorter distance may increase the thermal transfer from the hot electrode to cold.

While the space charge effect is comparatively less diamond materials due to its inherent NEA, its occurrence is significant enough that such implementation of remedies to quench this effect is still necessary.

Further remedies to reduce the influence of the space charge effect is the implementation of small external bias between the electrodes (~10V), Moreover, the addition of magnetic and electric fields between the electrodes can also reduce this effect. [50, 51]

Another drawback of TEC’s is the sustainability of the ultra-high vacuum (UHV) gap. UHV is necessary between the electrodes to prevent the collision of mobile electrons and gas molecules between the gaps. The potential scale up of such a device would mean more energy is necessary for produce a UHV, which reduces the overall efficiency of the device.

2- Diamond growth and development

2.1- Diamond synthesis history

2.1.1- discovery of HPHT and CVD

Due to diamonds natural scarcity, procurement and implementation of diamond into current technologies is not economically feasible in most situations despite the great potential benefits of its addition. A solution to commercial diamond procurement was invented in 1954 when Tracy Hall (known as the "father of the synthetic diamond"), who worked at General Electric at the time, invented a press which could repetitively produce the necessary conditions to form diamonds. The method Hall used is known as the High Pressure, High Temperature (HPHT) method for forming diamonds and can produce commercial scale volumes of diamonds. The Press he developed was able to sustain temperatures of 2,000°C and pressures of 10GPa.

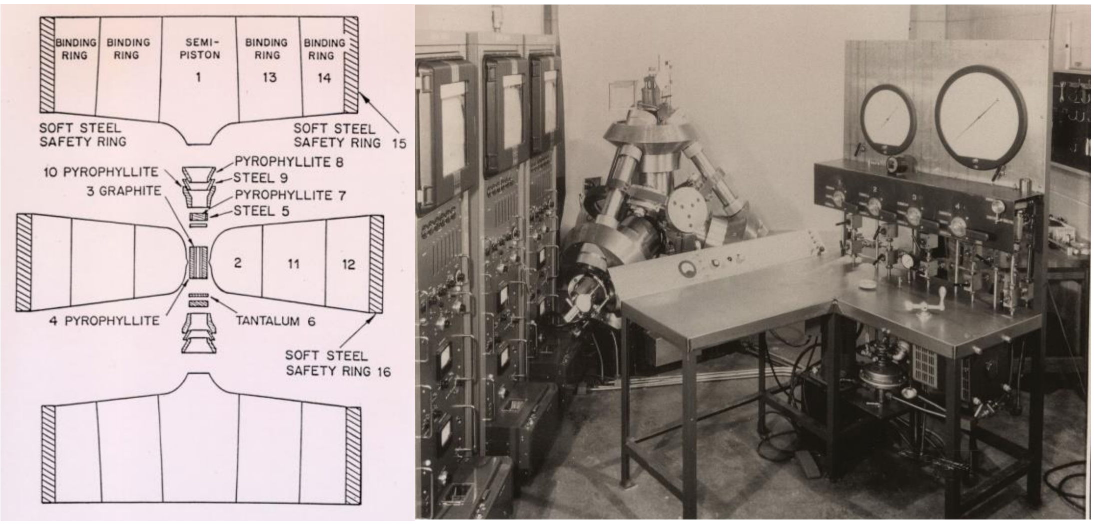

Figure 14: left) patent schematic of HPHT reactor, right) HPHT reactor in Tracy hall's lab

Since Hall's synthesis, there have been continuous developments within the field to improve the efficiency of diamond production. [52]

The HPHT method of diamond synthesis uses high temperatures and pressures to melt a metallic capsule comprised of a mixture of metals which act as a solvent-catalyst for the loaded carbon to both dissolve into and crystallise out of[53, 54]. Catalysts such as Iron, Nickel and cobalt are commonly used[55] however a variety of metals and materials have been reportedly used for the growth of diamond under HPHT conditions. [53]

During the same period which HPHT was discovered, the method of growing crystals at much lower temperatures and pressures was achieved in 1953 by William G. Eversole, however this benchmark in diamond synthesis was not published till 1962, nearly a decade later. This method used the pyrolysis of hydrocarbon gases onto a substrate, producing diamond growth. The CVD method produced by Eversole was reproduced by Angus in 1968[56] then subsequently replicated by Deryagin and Fedoseev in 1970. Deryagin and Fedoseev[57] later discovered that other substrates such as silicon can be used in place of single crystal diamond. The inexpensive nature of diamond growth on non-diamond substrates via CVD allowed for an increase in the amount of research potential within the field.

2.1.2- Unconventional methods

Less popular methods to produce diamonds are the ultrasonic cavitation method and the detonation method:

Ultrasonic cavitation uses the exceptional temperature and pressure differentials at the point of formation and collapse of a cavitation bubble to induce the conversion of graphite to diamond within an organic solution. For the production of diamond using this method, graphite is suspended in a solution comprised of an aromatic oxide oligomer CnHmOx (n = 18-36, m = 14-26, x = 2-5) [58] to a solid-fluid ratio of 1:6. An ultrasonic sound wave is induced onto the system, causing micro bubbles which, upon implosion, creates a brief window of ideal temperature and pressure conditions to transform the graphite to diamond. This transformation process is terminated once the pressure and temperature differentials homogenise between the point of implosion and the surrounding solution.[59]

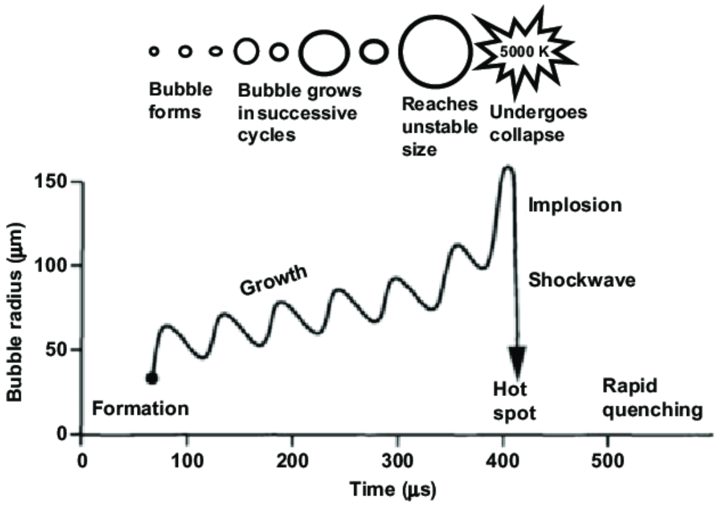

Figure 15: demonstrating the cavitation bubble cycle to progression of time [59]

Detonation synthesis of diamond uses the energy from an explosive detonation to drive the transformation of carbon to diamond. For this method, a vessel is loaded high yield explosive material and detonated in an oxygen free vessel. The resulting detonation causes an immediate rise in temperature and pressure, inducing the transformation of graphite to diamond crystals. Like the ultrasonic method, there is a short window in which the conditions produced from the detonation are favourable for diamond formation, which ultimately terminates from the consequential equalisation of surrounding temperature and pressure, the resulting diamonds are only ~5nm in size.[19]

Both methods are low yielding due to their inability to sustain the necessary conditions for diamond growth for long periods of time unlike the conventional methods, thus are sparsely used in both research and commercial settings.

2.2- CVD

In recent years, CVD has become the more favourable method for diamond growth due to several factors[60]: Growth rates of CVD reactors have increased greatly since their inception; This is due to more advanced method such as plasma assisted growth which both controls the uniformity of the dissociated carbon atoms crystallising out onto a substrate and making the carbon atoms more readily available to the growth substrate.

Generally, both methods are used however CVD has become favourable for the growth of gem quality diamonds, whilst HPHT diamonds are more commonplace for use in industrial applications.

CVD diamond growth is more favourable for solid state research however, due to the ability to control the amount of carrier gas going into the reactor chamber. This allows for sequential layering of different types of doped diamond, as well as direct control of the dopant concentrations in real time using the mass flow controllers (MFC). This gives rise to niche configurations of dopant diamond layers which can be studied/ characterised.

2.2.1- Mechanism

CVD diamond synthesis employs a gas phase reaction to activate carbon precursor molecules in an excess of hydrogen gas, which subsequently deposes on a substrate. An energy source (hot filament, microwave, torch) is used to induce a cascade of dissociation reactions within the carbon precursor, which prime the carbon for deposition. [44]

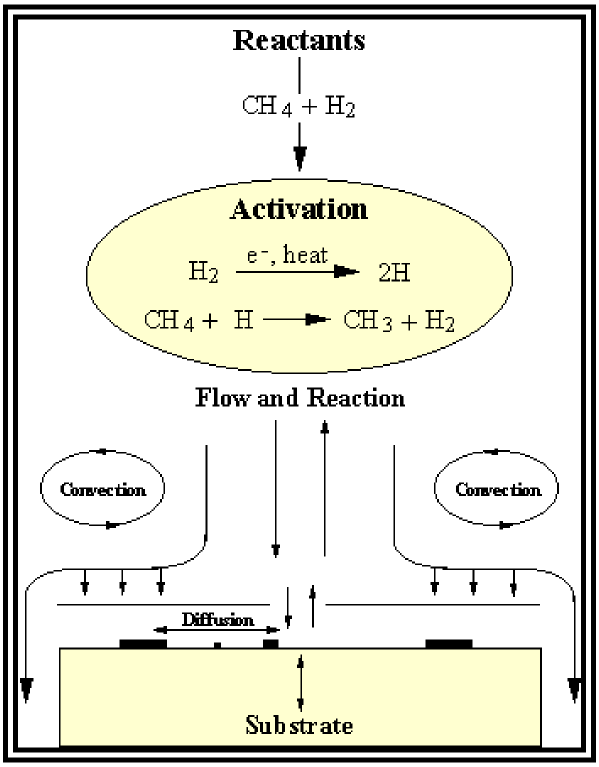

Figure 16: Illustration of the activation of gas species, with propagation to the substrate surface [61, 62]

The mechanism of activating the carbon precursor is an array of dissociation reactions which displace hydrogen from the initial carbon containing substituent gas, forming highly reactive methyl and hydrogen radicals that diffuse towards the substrate.

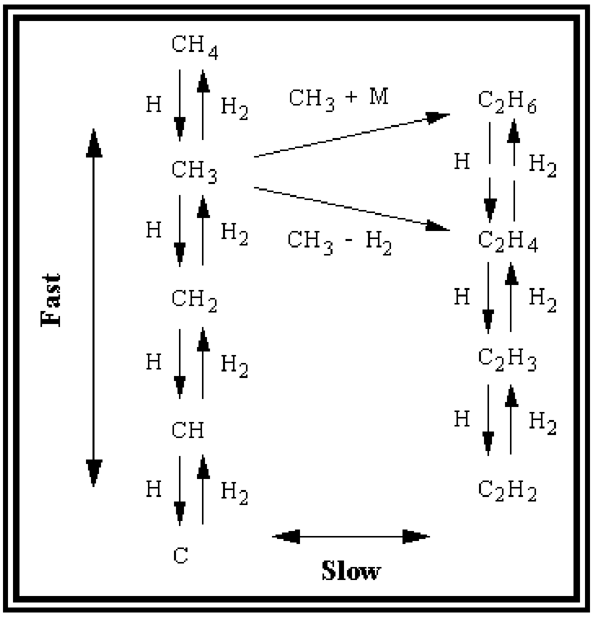

Figure 17: Dissociation reaction cascades between methane species and ethane species[62]

Hydrogen radicals cleave terminations at the diamond surface, leaving a vacant site for the carbon species to deposit onto the surface. This stepwise addition of methyl radicals builds up on the surface of the nucleated diamond, increasing the size of the diamond lattice. It Is necessary that during the activation of the carbon species, that the substrate maintains a temperature of 1000-1400K for diamond growth to take place.

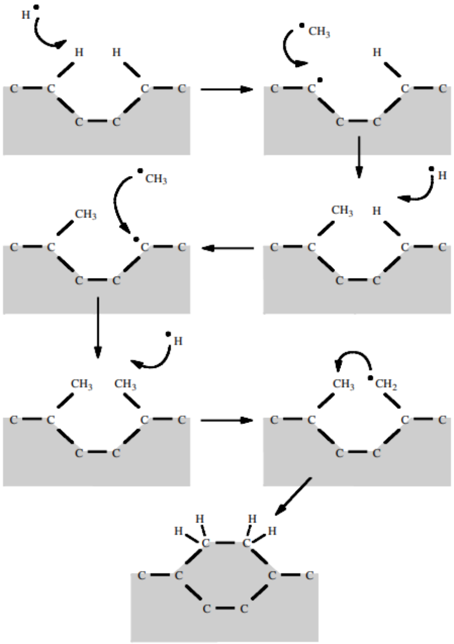

Figure 18: Illustration of the stepwise diamond growth process[44]

In summary, an equilibrium forms at the substrate surface when temperature and pressure is constant; For diamond growth, The rate at which carbon radicals perform the stepwise addition to the diamond nucleation sites must exceed the rate at which the hydrogen radicals cleave the carbon atoms from the surface. The greater difference between these two rates, the faster the growth of diamond on the substrate.

2.2.2- Common Setups

Different reactor configurations induce these dissociation reactions differently, and consequentially play a factor in the growth rate and quality of growth. The three common configurations for research scale growth chambers are hot filament, plasma and torch reactors.

2.2.2.1- Hot filament

this type of reactor employs a set of metal filaments that are situated above the substrate. The filaments are heated to thermally emissive temperatures by passing a current through them. Gas flow to the chamber passes through the array of hot filaments, forming the necessary radical species for diamond growth.

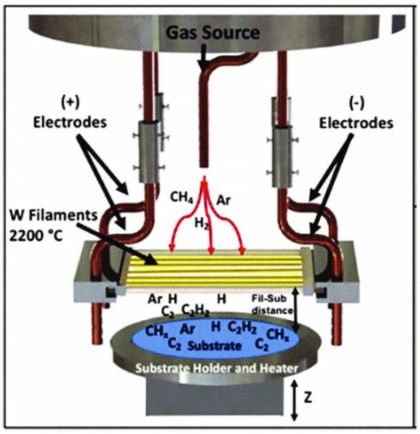

Figure 19: Schematic of hot filament reactor setup for diamond growth[63]

This method of thermally activating gas decomposition is simple to employ however has several drawbacks. Upon heating of the hot filaments, any tension within the wire when preparing the chamber can cause the filament to snap. Furthermore, the metal filaments at such high temperatures can potentially eject some of the metal from the surface, causing contamination of the diamond growth[64]. Additionally, If the samples are not placed directly under the filaments, growth fluctuations can occur across the sample surface.[63]

2.2.2.2- Plasma torch[65]

Plasma torch configuration employs a nozzle for gases within the reaction chamber. The torch is equipped with a microwave generator connected to the gas feeding tube. The reactant gases used for the chemical vapour deposition of carbon radicals is fed through the nozzle, upon reaching the region affected by high power microwave radiation, the atoms constituting the gas dissociate into a state of plasma. The gases maintain a state of plasma upon leaving the nozzle, creating a plasma torch. Research by K.F. Sergeichev *et al.* in 2009 demonstrated a growth rate of 3 microns per hour for polycrystalline diamond growth.

2.2.2.3- Microwave assisted plasma

Microwave is a commonly employed method for diamond synthesis. The benefit of plasma assisted methods is the ability to concentrate the plasma produced directly above the substrate. Such positioning allows for the substrate to be heated and sustained to temperatures whilst also activating the carbon precursor for deposition. This configuration was utilised for the project, thus will be elaborated on further.

2.2.3- MPCVD

The key component that drives the microwave reactor's operation is the magnetron. The magnetron uses a high electric current through a magnetic field to produce a microwave radiation. The emitted microwaves travel through a waveguide tunnel towards the reactor chamber and sample holder. [66]

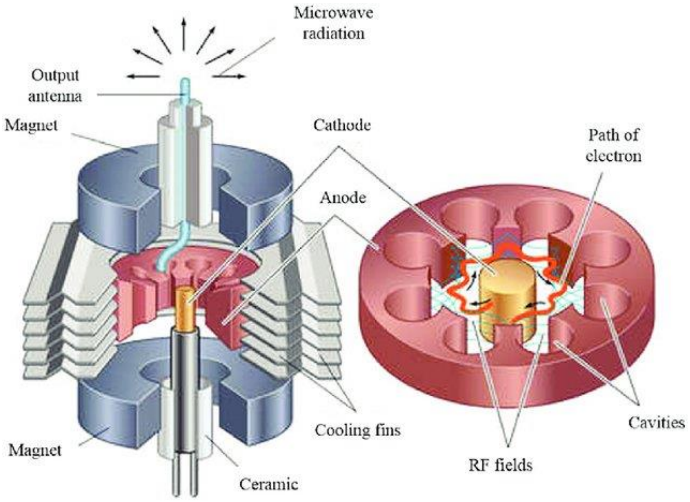

Figure 20: the design of magnetrons used for microwave production in CVD chambers[66]

The waveguide tunnel is equipped with 3 impedance tuners, which can be used to vary the power transmitted to the chamber. These tuners can be manually adjusted and, when the source and load impedance matches, 0 wave reflection occurs, thus no observed power loss (reflective power) should be observed and all energy generated should be fed towards the reactor chamber (forward power). This maximum power transfer theory is defined by Jacobi's law [67], where a change in the source impedance can change the impedance in the load (in this case, the reactor chamber).

To induce plasma within the reactor, the chamber must initially be purged of air, then backfilled with a hydrogen gas flow, to which the plasma will be struck. The input of plasma to the hydrogen rich environment produces ionised atoms. These ionised atoms have the potential to recombine back to hydrogen. The rate of the ionization to recombination much greater, thus a sustained breakdown via the energy induced by the microwave radiation creates a gas mixture of ionised protons and free electrons, this is known as thermal plasma, where the temperature of the ions and electrons are approximately similar ($T_e \cong T_i$).

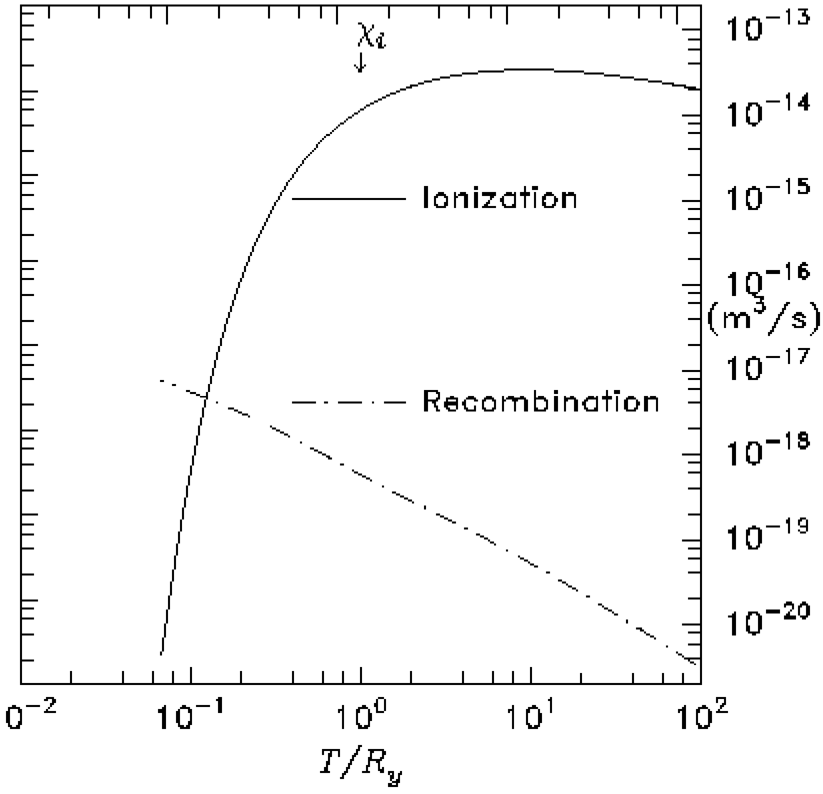

Figure 21: Graph illustrating the ionisation and recombination of microwave plasma

The size of the plasma is affected by three key factors, The microwave energy input, the temperature of the plasma, and the pressure of the chamber. Furthermore, the colour of plasma varies depending on the gases contained in the plasma; Pure hydrogen gas gives off a purple hue, a characteristic from its primary and secondary emission lines of wavelengths 656.3nm and 486.1nm respectively. This colour is also characteristic of gas with low concentrations of plasma.

Once the plasma has established, concentrated above the substrate and raised to the relevant power value, the introduction of the carbon substituent gas (typically methane) and other dopant gases can occur. The Secondary gases added constitute a much lower concentration of the plasma, with the ratio of hydrogen to methane generally being ~30:1, and the ratio of dopants such as boron being 300:1.[68-72]

The Prominence of hydrogen gas and its radical constituent form is pertinent to the development of diamond crystals in all CVD setups. This is due to it performing several functions in the growth process, such as terminating dangling bonds at nucleation sites, stabilising the diamond surface, as well as selectively etching graphic phase carbon and creating radical sites via hydrogen abstraction.

During the period between striking the hydrogen gas flow with plasma, and introducing the carbon gas, Hydrogen radicals cause surface etching of the substrate. This is beneficial for short periods of time as potential oxide species residing on the substrates surface layer are removed [73]. [74] During the termination of the diamond growth, hydrogen plasma begins to etch at surface defects, decreasing surface roughness. However, studies by Jiang et al. showed that prolonged surface etching concentrates at grain boundaries, causing reemerging surface roughness. Furthermore, the diamond surface, when terminated with hydrogen, gives rise to the characteristic NEA of diamond film[75].

2.2.4- Dopant gases

Like methane gas, gaseous dopant species are used to produce the atomic radical species necessary for the doping of diamond film. The carrier gases used are the sources of the dopant atoms intended for incorporation within the diamond lattice. This is due to some species being more easily dissociable into their constituent atoms.

The concentration of reactant gases plays a crucial role in the surface morphology of the diamond growth, such as the prevalence of specific orientations on the diamond surface; High concentrations of methane are attributed to increased populations of [100] and [111]. This effect is coupled with the variation of growth temperature; thus, both must be regulated[76].

2.2.4.1- p- dopant gas

Boron is the most common P type dopant incorporated into the diamond lattice. In terms of the carrier gas used to produce the atomic species of boron, the most prominent gas species used is diborane. [61, 62, 77, 78]

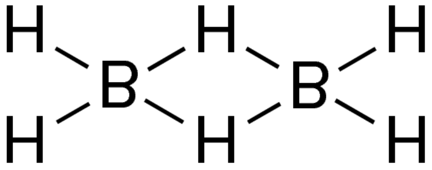

Figure 22: Diborane chemical structure

With the addition of these dopants into the gas mixture during diamond growth, new radical species form which introduce the dopant species into the grown diamond, while also producing less desirable radical species. Alternative doping species have been used with varying results, as the case of trimethyl borate, which showed preferential incorporation within [111] growth orientations yet had a lower B/C ratio than that of the gas phase. [68, 69, 79]

A key factor to consider when introducing boron composed gases to the CVD chamber is their interatomic interactions with other gas species. Experiments involving boron doping indicates the potential production of soot that greater concentrations/flow rates of boron carrier gases, consequentially hindering the growth process. This soot production is characteristic of growth in high density microwave plasma reactor setups [25]. The production of soot is also characteristic of high H_2/CH_4. [70]

2.2.4.2- N-dopant gases

A variety of N type dopants are commonly incorporated into diamond film, the most popular being Nitrogen and phosphorus. Nitrogen is commonly incorporated into diamond using its molecular gas species, however there are drawbacks using this as the carrier gas. The primary reason being the bond strength on nitrogen gas (946KJ/mol). This mean radical constituents of nitrogen for surface adsorption are less prominent. Alternative carrier gases have been explored for nitrogen doping, such as the use of nitrous oxides[80]. Experiments conducted by M.Ngambou *et al.* Demonstrated the use of N_2O as a dopant gas to improve the density of nitrogen vacancy centres in diamond film growth. Furthermore, the researchers showed that lower methane concentrations and temperatures enhanced NV doping.

Figure 23: chemical structures for left) Nitrous oxide, right) Nitrogen gas

the usage of different carrier gases in H_2/CH_4 plasma can produce side reactions upon their introduction to the plasma. For example, the use of phosphine gas in plasma for doping diamond dissociates into simple phosphorus radicals (PH and P), which can then undergo either a stepwise addition onto the diamond lattice, or react with methane in the gas mixture, producing methyl phosphine. [79, 81, 82]

2.2.5- Substrates

2.2.5.1- Selection & orientation

Three parameters which govern the feasibility of a given substrate for diamond growth is as follows: the substrate must be able to withstand high thermal stress, it must also be able to withstand attack by the activated gas species and not dissolve the carbon into its lattice. A variety of substrates adhere to these parameters thus are used frequently in diamond growth. These range from crystalline species such as single crystal diamonds, silicon (pure, carbide and nitride forms), quartz glass and cemented carbides, to metallic species such as tungsten, molybdenum, iridium and their oxides. [83]

Different feasible substrates are employed depending on the application of the diamond film, in the case of nitrogen doped diamond, silicon [100] is commonly employed due to the improve crystal quality of grown diamond[72]. Furthermore, some substrates are used more readily due to their availability, scalability, thermal expansion and similarity to the diamond lattice structure.[77]

In the case of nitrogen doped diamond growth, three parameters dictate the rate of growth: Substrate temperature, Methane concentration and nitrogen concentration in gas phase. O.Brinza et al. Performed computational studies, varying the dependence of these parameters, showing the greatest increase in growth rate from diamond substrate orientation [110] with the increase of all three parameters exclusively. Moreover, in all cases, [113] orientated diamond showed the slowest growth rate of all the orientations used [84]; These results were consistent with experimental observations.

In terms of these thermionic emission investigations, Molybdenum substrates will be used due to its high melting point temperature, it's inertness to the activated gases during the deposition process, high thermal conductivity and its thermal expansion coefficient being like CVD diamond[77]. Furthermore, it's reported that initial diamond nucleation in plasma reactors produces a carbide layer on the substrate surface, followed by diamond like carbon that quickly changes bonding structure from sp2 to sp3, enhancing the rate of diamond nucleation. [85]

2.2.5.2- Nucleation

CVD techniques for the growth of diamond film require pre-existing nucleation[86] of powdered diamond to induce crystal growth within the CVD chamber. There are two techniques which are commonly employed to pre-treat a substrate with diamond.

The most common method of substrate treatment is the manual abrasion of diamond powder onto the substrate. This method uses shear stress to embed the diamond powder onto the surface, creating a buffer layer of nanocrystalline diamond which diamond growth can take place from. The benefits of this method of nucleation are twofold. The method is inexpensive, only requiring the rubbing to two wafer substrates with the diamond powder in between. Secondly, the shear stress from the diamond being compressed and scraped between the substrates introduces surface defects where the diamond powder can embed, improving surface adhesion of grown diamond later. The one drawback of this method is the mechanical stress on the substrate can potentially bend it. Moreover, an even distribution of nucleated diamond cannot be guaranteed.

The alternative method for the nucleation of the substrate is the electrospray deposition method of adding diamond nanoparticles to the substrate [87]. The preparation of this method involves the suspension of the diamond powder in a solution of methanol. When added to the solvent and placed in an ultrasonic bath, the diamond powder disperses through the solution to form a colloidally stable solution. The substrate is then attached to a spinning disk electrode, with an electrospray nozzle containing the colloidal solution being aimed at the substrate. When a current is passed through the nozzle, A fine dispersion of the colloidal solution travels to the disk, evenly distributing the suspended diamond onto the substrate. This method ensures an even distribution of the diamond powder onto the substrate; however, the lack of deeply embedded diamond can cause delamination of the diamond film after diamond growth occurs.[88]

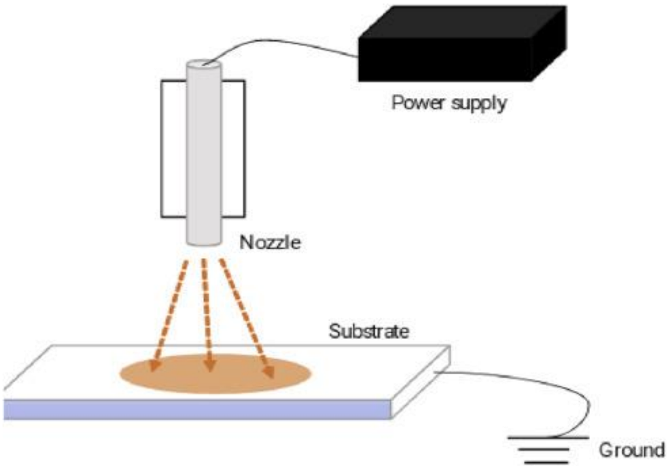

Figure 24: schematic of an electrospray nozzle for substrate nucleation[88]

2.3- Dopant effects on diamond films

2.3.0- Band gap size and implications

The addition of dopants is fundamental for mobility of electrons within diamond. The presence of dopants in diamond's crystal lattice alters the band structure of diamond, changing the position of the fermi energy and subsequently the band gap, ionisation energy and work function. Varying both the presence of given dopants and their respective concentrations allows for the engineering of diamonds band structure to perpetuate the emission of electrons from the bulk lattice to vacuum. The addition of different N type and P type dopants can introduce donor and acceptor levels respectively.

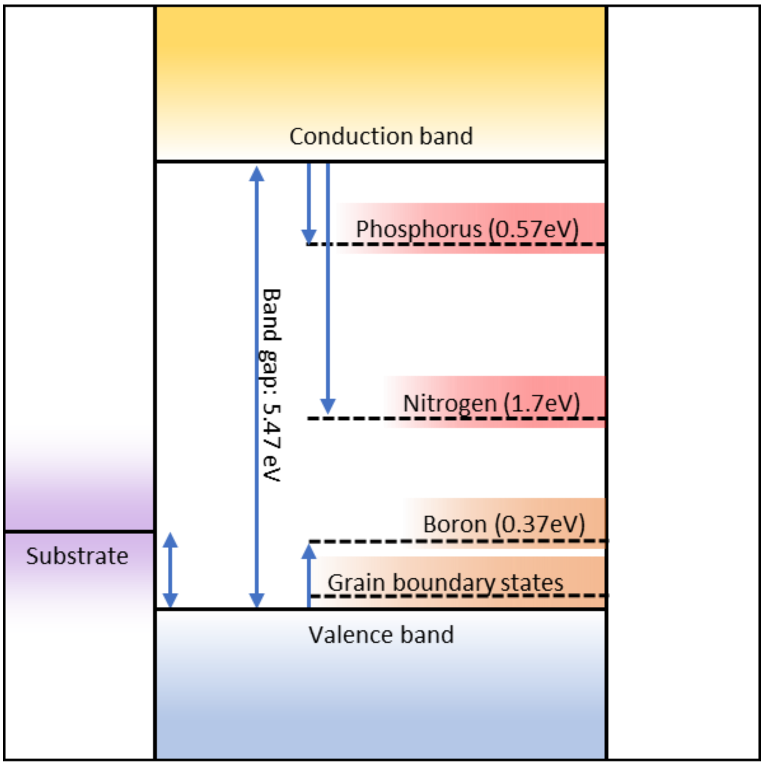

Figure 25: adapted image of N and P type dopant levels, with grain boundary state level

2.3.1- N type doping

N-type doping of diamond substrates incorporate atomic species with a surplus of electrons in the diamond lattice. In terms of band structure, n dopant levels lie below the conduction band minima. As these new energy states are populated with electrons, the fermi level is raised.

For application within thermionic emitters, dopant species with shallow doner levels are more desirable, as their energy is situated closer to the vacuum level of the diamond surface, making them energetically favourable.

For n-type dopants, nitrogen is the most commonplace dopant for diamond growth[1, 77, 78, 80, 84, 89-99]. Several factors favour its incorporation compared to other n-type dopants. Nitrogen's atomic size is comparable to carbon, thus its substitution into the diamond lattice has little effect on the structural properties of diamond, whilst simultaneously improving the concentration of charge carriers within the system.

For nitrogen, the bonds formed with the surrounding diamond structure causes partial distortion which generates a deep doner level. This is due to the preferential lone pair bonding to the nitrogen atom, leaving a dangling bond with one of the four carbon bonds. This deep donor level becomes more pronounced at greater concentrations.

Dopant defects which include interstitial Hydrogen partially mitigates this by residing in the space of the unsatisfied valence, relaxing the state of the nitrogen and reducing its dopant level slightly[91].

While phosphorus has desirable characteristics of a donor species due to it being a shallow donor, incorporation of it within the diamond lattice is a greater challenge compared to nitrogen, primarily due to its atom size. A variety of experiments have studied both dopant species with different substrates.

In terms of diamond growth, studies monitoring the growth of diamond with the addition of nitrogen has shown an increase in diamond growth rate[93]. Moreover, addition of nitrogen is observed to increase the size of diamond crystallites[92, 93].

2.3.2- P type doping

P type dopants are electron deficient atomic species incorporated within a lattice. The introduction of p type dopants produces conduction states that reside close to the VBM. As valence electrons can “jump” to these available states, doping using p type elements shifts the fermi level to that greater than undoped diamond.

Boron is the most employed dopant for similar reasons to nitrogen; Its atomic size is comparable to that of carbon thus its incorporation into the lattice is relatively straightforward. Extensive research shows the linear increase of conductance within diamond relative to concentration increase.

Few other acceptor species have been experimentally implemented within diamond’s lattice. Select computational studies using density function theory (DFT) have incorporated transition metals as acceptor species[100].

An aspect of p type doping that is unfavourable in terms of conduction and emission of electrons is the passivation of acceptor species. Passivation occurs when hydrogen species occupy the vacant site of boron within the diamond lattice. This occurs due to hydrogen can quickly diffuse into the p type lattices, immobilising electrons and reducing conductivity. Luckily, this can be mitigated using low pressures and/or high temperatures that can desorb the hydrogen from the bulk lattice[101].

2.3.5- Substitutional and interstitial doping

A notable aspect of diamond doping is the positional effects of dopants. For monoatomic dopant species, their positioning within the lattice has a profound effect of the fermi level of diamonds band structure. Work from D.Zhou et al. demonstrates that interstitially situated atoms vastly increase the fermi energy when compared to their substitutionally added counterparts[94].

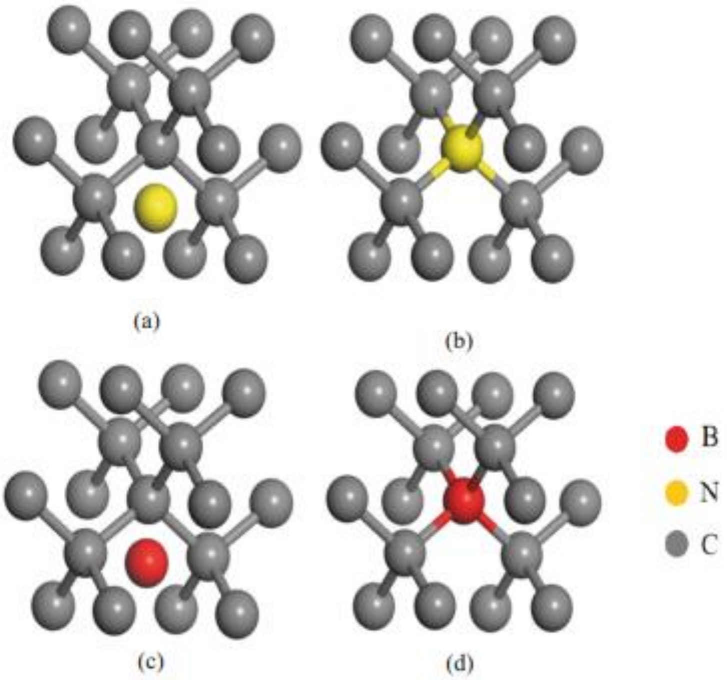

Figure 26: substitutional and interstitial Bonding configuration of a-b) Nitrogen, c-d) Boron[94]

2.3.3- Co dopant systems

Co doping is the addition of two or more dopant species within structure of a bulk crystal lattice. This primary need for co-doping within diamond is to produce a doner species within the diamond lattice that is shallower than conventional donors such as phosphorus and nitrogen, making for a better N type semiconductor. Examples of this is a first principles study by D.Segev in which the incorporation of Silicon-Nitrogen complexes was studies. Structures where silicon surrounds the nitrogen, was theorised to push the donor level of the nitrogen dopant to a greater energy, making it a shallow dopant[102]. At greater atomic volumes during modelling the complex was situated close or deeper in energy than phosphorus doping.

There are several drawbacks to the use of co doped species within diamond, for example, the localised structures involving the co dopants can vary drastically, giving rise to various degrees of donor/acceptor levels. This variation is statistical in nature, thus alteration of the parameters used to incorporate the dopants may allow for the favouring of specific structures[94].

2.4- Diamond surface modification

Bonding which occurs at the diamond surface can vastly affect the emission properties of diamond, making it a focal point of thermionic research. Upon growth CVD diamond, the outmost carbon lattice is abundant in vacant sites, which are energetically unstable. The diamond surface instability can be mitigated via two methods: reconstruction of the diamonds vacant surface to lower energy configuration can occur. Alternatively, the addition of termination species can stabilise these vacant sites. The bonding between the carbon and terminating species can vastly alter the electronic properties at surface level. This occurs due to the dipoles formed between the surface boundaries.

2.4.1- Lattice-Surface interface

The presence of hydrogen ions produces a dipole at the C-H boundary, causing downwards band bending, increasing the fermi energy and subsequently decreasing the work function of the diamond material at surface level.

Hydrogen terminations are the most accessible surface termination, being the standard termination species present for studies of doped diamond films. This is due to the use of hydrogen plasma during diamond growth. Upon completion of diamond growth, hydrogen atoms from the remaining plasma stabilise the dangling bonds of the diamond surface. For the outermost carbon atoms on the diamond lattice. Hydrogen terminated diamond film exhibits negative electron affinity, reducing the work necessary for electron emission. Application of hydrogen based thermionic emitters is restricted however, due to hydrogen's tendency for desorption from the surface at high temperatures.

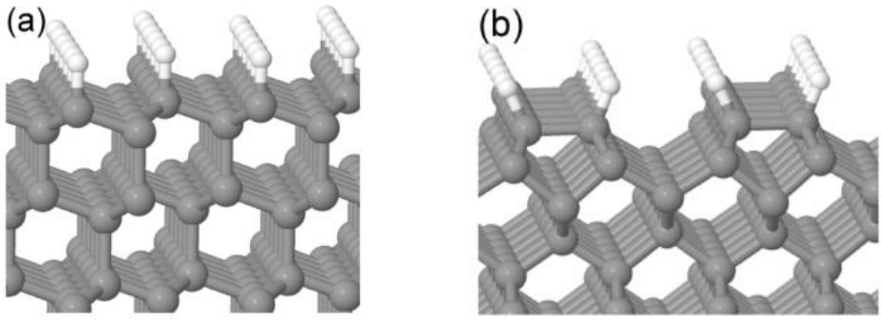

Figure 27: Hydrogen termination of a) (111), B) (100) diamond surfaces

For divalent or metallic species, the bonding to the diamond surface can vary. For example, Oxygen, a divalent atom, can exhibit 3 bonding motifs: That of ketone, Ether and alcohol. The prevalence of a given oxygen motif on the diamond surface is dependent on the termination technique used. Consequentially, the different types of bonding give rise to a difference in surface work function depending on the relative populations of oxygen motifs on the diamond surface[103].In terms of thermionic emission, oxygen terminations are unfavourable due to oxygen producing a positive electron affinity surface, raising the energy necessary to liberate electrons from the surface. Subsequent layering of metal terminations after oxidation of the diamond surface maintains the NEA needed for efficient electron emission while improving the bonding between diamond and the terminants added.

2.4.2- Surface terminations and work function

Extensive theoretical studies on diamond terminations have been recorded in literature:

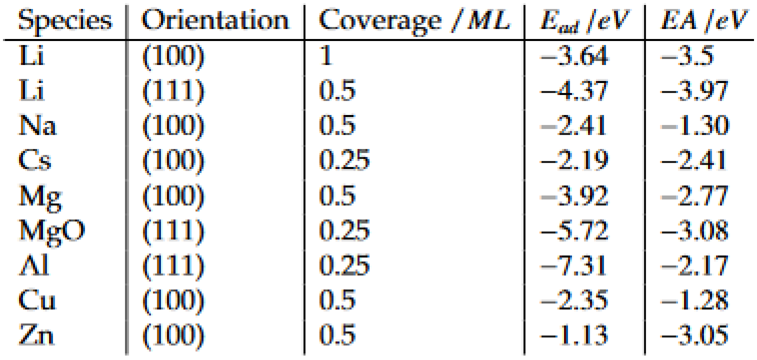

Species	Orientation	Coverage /ML	E_{ad} /eV	EA /eV
Li	(100)	1	−3.64	−3.5
Li	(111)	0.5	−4.37	−3.97
Na	(100)	0.5	−2.41	−1.30
Cs	(100)	0.25	−2.19	−2.41
Mg	(100)	0.5	−3.92	−2.77
MgO	(111)	0.25	−5.72	−3.08
Al	(111)	0.25	−7.31	−2.17
Cu	(100)	0.5	−2.35	−1.28
Zn	(100)	0.5	−1.13	−3.05

Table 1 : List of theoretical adsorption energies of metal terminants on undoped diamond, recovered from Rae-Darcia Holmes[77]

Two promising metal terminations for improved electron emissions are lithium and magnesium. In both cases, their low atomic mass makes their addition to the diamond surface relatively feasible. Both species have been observed to sufficiently increase the NEA of the diamond surface and reduce the work function. Like hydrogen, they both are limited to the temperatures they can operate at due to surface desorption. Experimental work performed by Rae-Darcia Holmes observed the emission current of Lithium oxide terminations on nitrogen doped diamond, showing a thermal activation temperature of ~650C and emission currents of 1 and rising to 1.5 through emission cycles. It was noted that the smooth currents formed were likely resultant of a relatively uniform surface.

2.5- Depositing terminations

2.5.1- Surface Oxidation

The oxidation of the diamond surface can be performed by a variety of methods. In terms of the bonding structures on the diamond surface, the method which oxidation occurs can influence the structural population on the film. In terms of the work performed in this project, UV-ozone was utilised. This method of oxidation is relatively straightforward and quick at producing an oxygen terminated surface. In terms of how the oxygen is added to the surface, the use of a mercury filament lamp induces radical dissociation of molecular oxygen bonds, producing radical species which can attack the diamond surface. The mechanism of this radical dissociation is as follows:

$$O_2 + hv \rightarrow 2O^{\cdot}$$
$$O_2 + O^{\cdot} \rightarrow O_3$$
$$O_3 + hv \rightarrow O^{\cdot} + O_2 \tag{18}$$

2.5.2- Ultra-high vacuum deposition

The addition of single layer, metal terminations is performed using ultra high vacuum. The deposition chamber used utilises current through a metal filament to induce evaporation of metal atoms at the materials surface, in which it travels towards the diamond sample and bonds to the sample. This method of deposition is optimal as it allows to produce fine atomic size thickness films.

2.5.2.1- UHV chamber

The Ultra high vacuum scale defines ranges of pressure below 1x10-6 pascals. At such pressures, any gas remaining has little intermolecular interactions from one another, thus atoms within the system have free molecular flow. To reduce fluctuations of pressure within the chamber, the chamber under pressure must be baked at high temperatures to cause outgassing of all surfaces within the chamber. Outgassing is the removal of surface bound gas molecules within the chamber, that can be removed via low pressures or high temperatures.

In terms of surface terminating the diamond sample for the project, low pressures are necessary to prevent any stray gas particles from obscuring the sample surface from the ejected metal atoms.

2.5.2.2- Filament evaporation

To terminate the diamond sample with metals, a filament of the metal used for termination must be placed next to the sample with the diamond surface facing the filament. Like the chamber, the filament and sample must be pre-annealed to ensure all bound gas molecules are removed from their surfaces.

For terminating metal onto the surface of the diamond, a current must be induced on the filament, causing heating. The heating of the filament is proportional to the current induced, thus raising the current allows the filament to reach a temperature which ejects the hot metals atoms off the filament surface. In UHV conditions, ejected metal atoms diffuse to the cold diamond surface to evaporate, adhering to the diamond surface.

In terms of lithium deposition, 1.5 minutes is needed to evaporate enough metal to form a full metal layer on the diamond surface.

2.5.3- Absorber surface alteration

In a thermionic device, the back end of the substrate diamond is grown is used to absorb energy from a light or thermal source. Optimisation of the absorber surface is essential to supplying energy to the emitting diamond surface. Two methods have been utilised previously to produce a more absorbant surface.

Diamond-like carbon

By altering the parameters used for deposition within MPCVD, a film of amorphous, glassy carbon is deposited onto the back end of the emitter substrate.

Parameter	Value
Methane	25sccm
Hydrogen	300sccm
Nitrogen	1.5sccm
Pressure	140Torr
Power	1.5kW
Temperature	1200C
Time	3 hours

Table 2: Synthesis parameters for diamond like carbon; performed by Rae Darcia Holmes

When comparing DLC conditions to standard diamond growth parameters, we see a ~10-fold increase in the concentration of methane added to the system. The additional carbon concentration results in a greater proportion of graphitic species being formed form the growth, producing an amalgam of sp_3 and sp_2 carbon structures which can better absorb radiation than the conventional molybdenum surface.

Laser etched gratings

The use of gratings on the molybdenum surface has been observed to increase the thermal absorbance of the substrate by 90%. The gratings are fabricated using a high-powered laser to etch parallel lines separated by 10.5 microns. The addition of the micron sized gaps produces a characteristic matte back surface which efficiently absorbs visible light. For the project, laser gratings were employed on the absorber surface of the samples produced.

3- Experimental

3.1- Sample preparation

A total of 6 growth runs were performed on the MPECVD reactor within the University of Bristol diamond lab. Initial growth runs on silicon were performed to determine the growth rate of boron doped diamond within the reactor. Further growths on molybdenum diamond film with boron and nitrogen doping were later fabricated and used for thermionic studies.

Substrates were manually abraded with diamond nanoparticles. The substrates begin as reflective materials, which upon nucleation of diamond, gives a grey, opaque hue. A swab is saturated with isopropyl alcohol and rubbed on the nucleated surface to remove loose nanoparticles from the abraded surface. This prevents the growth of clustered diamond on the growth surface.

The reactor is opened to atmospheric pressure via the valve highlighted yellow. A 0.5mm molybdenum wire and disk is centred on the baseplate of the reactor chamber, with a sample placed on top. The stage of the reactor is then moved to isolate the chamber, with the valve for air being closed and the one to pump opened. The water and air coolant systems are enabled for both the reactor and magnetron.

Figure 28: MPCVD setup, annotated

chambers pressure is reduced to 5x10^{-5}pa, to which the hydrogen gas line is enabled on the mass flow controller on the rack (gas flow set to 300sccm for all runs). On the rack, the pressure of the vessel is stabilised to 15 torr before striking the hydrogen gas with plasma (starting with ~0.64 MW). The pressure and power are then raised to the conditions outlined in 3.1.1 & 3.1.2, with the methane and dopant gases being added at their respective concentrations at a pressure of 50torr. During this increase, the tuning rods are manipulated to minimise the reflective power of the produced microwaves. The temperature of the sample is measured via a pyrometer attached to the reactor setup and is displayed on the rack, The emissivity of 0.19 and 0.18 was set on the display for silicon and molybdenum respectively.

3.1.1- calibration growth

The initial calibration growth of boron doped diamond was performed using the following parameters:

Parameter	Value
[Methane]	1.5sccm
[Hydrogen]	300sccm
[Diborane]	2.1sccm
Pressure	140Torr
Power	1.5kW
Temperature	~950C

Table 4: calibration growth parameters

2 calibration growths were conducted using diamond nucleated (111) silicon, with the above setup described in 3.1 performed each time. The intervals for growth were of 1 and 2 hours starting from the stabilisation of the temperature and power used. Upon completion of growth on each sample, thickness of the growth was recorded by breaking the sample in half using a diamond scribe and observing the width of the snapped cross section under Scanning electron microscopy. From this, a plot of film thickness relative to time can be produced. It is extensively reported that growth rates of diamond films follow a linear pattern, thus the two runs can be extrapolated to determine the growth rates of longer deposition times.

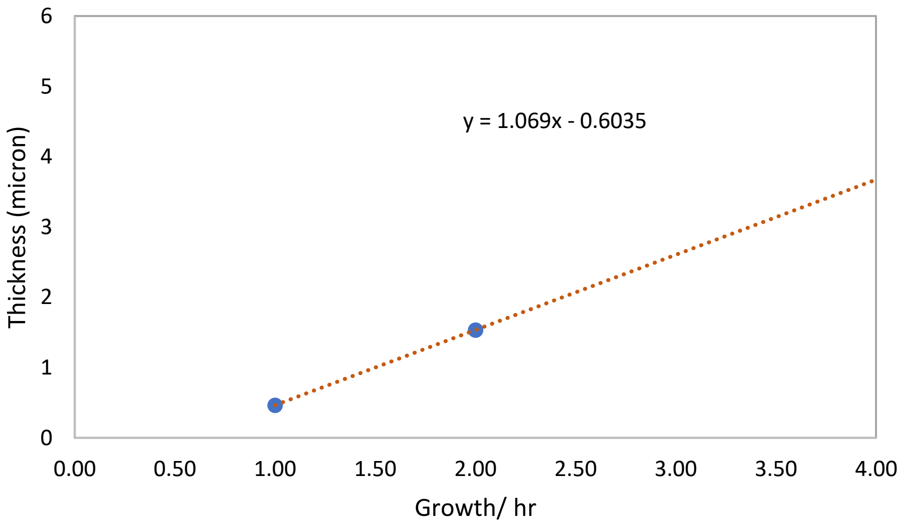

Figure 29: calibration growth runs plotted against thickness

Observing the calibration plot, we can identify that the initial data point's calculated thickness is limited. This is characteristic of diamond growth; as growth sites become established, the growth rate becomes linear.

3.1.2- BNDD growth

3 growths of boron-nitrogen doped diamond films were fabricated with identical parameters for growth. The initial 3 hours of growth employed Diborane gas to produce a p-type diamond film, to which the dopant gas is replaced with nitrogen for the final hour:

Parameter	Value
[Methane]	1.5sccm
[Hydrogen]	300sccm
[Diborane]	0.5sccm
[Nitrogen]	1.1sccm
Pressure	140Torr
Power	1.5kW
Temperature	~950C

Table 5: BNDD growth parameters

Despite identical conditions being used for growth of the diamond film, observation of the final growth run showed a region of significant difference in colour compared to the first two growths: a circular spot of darker film covering a third of the sample surface. Subsequent analysis of the samples outlined in section 3.2.1 and 3.2.2 shows significant difference in structure of the diamond film, hence further analysis was terminated for BNDD-3.

3.1.3- Sample oxidation

BNDD 1 and 2 were oxidised in preparation for lithium deposition using the UV-Ozone generator within the Bristol electrochemistry lab. The ozone generator functions at room temperature an ambient pressure. BNDD-1 and 2 were placed in the generator for 30 minutes to produce an oxidised surface layer.

3.1.4- Lithium termination

Lithium deposition onto BNDD-1 and 2 was performed in the deposition chamber of the NanoESCA, a versatile machine used for both deposition and photoemission analytical techniques used before and after deposition steps.

[insert nanoESCA image]

The samples were mounted and secured on slides used to manoeuvre the sample throughout the UHV chambers. For sample loading, a chamber containing a wobble stick with loading slots is brought to atmospheric pressure. The sample are then loaded, the chamber isolated and pressure reduced to UHV conditions. For the transfer of the sample from the loading chamber to the deposition chamber, the pressure within the loading chamber is brought to 1x10-7pa, this is to ensure that no significant fluctuation of pressure occurs upon movement of samples from one chamber to another.

To remove contaminants from the surface of both the filament and sample, pre-annealing is performed. For the loaded sample, the stage which it is situated on is gradually heated to 300C (max pressure reached from outgassing: $1x10^{-6}$ mbar), where the sample is allowed to outgas weakly bonded surface contaminants for 1 hour. A current of 2.7A with a voltage of 2.5V is applied to the lithium filament, heating it to 439C. The temperature and pressure ($3x10^{-8}$ mbar) are maintained for 15 minutes, ensuring all contaminants are removed.

The sample is then positioned aside the filament, with the diamond surface facing it. The following parameters were used for the evaporation of lithium onto the diamond film.

Parameter	Value
Temperature	440C
Current	2.7A
External voltage	2.6
Background pressure	$3x10^{-9}$mbar
Deposition pressure	$3x10^{-8}$mbar

Table 6: parameters for lithium deposition

The parameters used for deposition were pre calibrated from recent deposition experiments [77].

Upon analysis, BNDD 1 was observed to contain lithium on the surface (section 3.2.2). BNDD 2 was unable to undergo termination of lithium due to dislodging from the sample stage within the deposition reactor.

BNDD 1 was transferred from the deposition chamber to an adjacent analysis chamber for post-anneal treatment. The use of annealing after deposition allows for the surface reconstruction of lithium to promote bonding between the lithium and oxygen layers on the diamond surface. The anneal treatment was performed at temperatures of 500C for 1 hour.

3.2- Analysis

3.2.1- Surface quality

3.2.1.1- Raman spectroscopy

Initial analysis of hydrogen terminated BNDD samples (henceforth referred to as H-BNDD) utilised Raman spectroscopy to briefly analyse the bond structures present on the diamond surface [104]. For Raman analysis, the incidence laser interacts with molecular vibration within the diamond lattice. Upon relaxation, and photon of greater wavelength is re-emitted. The difference in wavelength (known as stokes shift) is plotted the form of wavenumbers. Diamond has 3 characteristic peaks that occur during Raman spectroscopy, which can be used to determine the surface structures of the samples. For recording of spectra, 15 frames of 10 second exposure time was taken at 60% laser power.

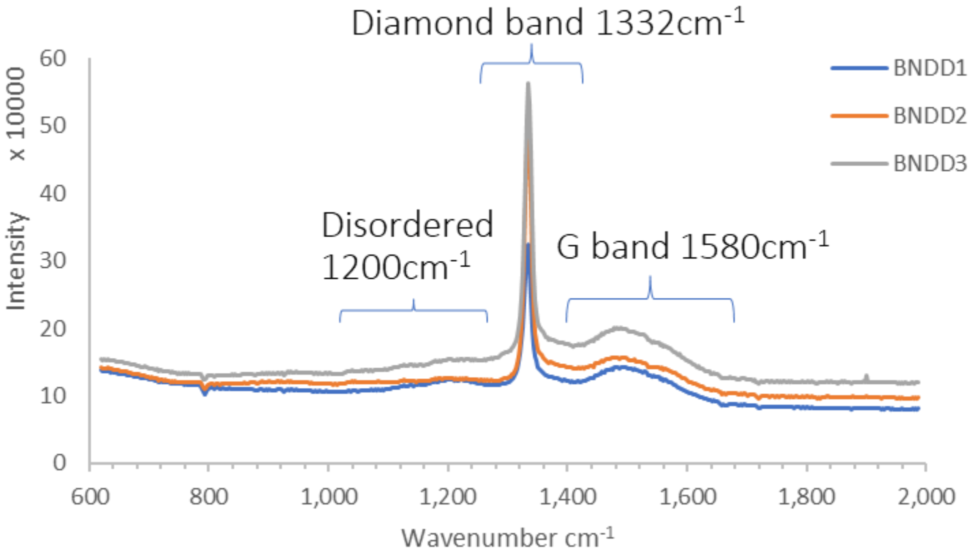

Figure 30: Raman spectroscopy of BNDD samples

The resulting plots from Raman spectroscopy of the 3 show the prevalence of Sp_3 carbon structures on the surface of the material, this is representative of the 1332cm^{-1} peak in the centre of the plot. Furthermore, the D-band, where disordered carbon can be identified is absent of any significant peak. Primarily, the D-band peak is indicative of boron surface doping. Absence of this peak signifies lack of migration of boron species to the surface layers.

The G-band region is characteristic of graphitised surfaces. From the spectra taken, it is apparent that H-BNDD 3 has a greater population of graphitised species, which may explain the defect observed on the surface.

3.2.1.2- Scanning electron microscopy

Scanning electron microscopy (SEM) utilises an electron beam to bombard the diamond surface with electrons. The bombarded material produces secondary electrons which can be detected, to which an image showcasing the topography of the material surface is produced.

It is recorded that species with NEA, or electropositive surface dipoles produce a brighter images, as the proportion of secondary electrons from these regions are greater. Conversely, electronegative species are observed as darker regions on the produced image. H-BNDD 1-3 were all analysed via SEM.

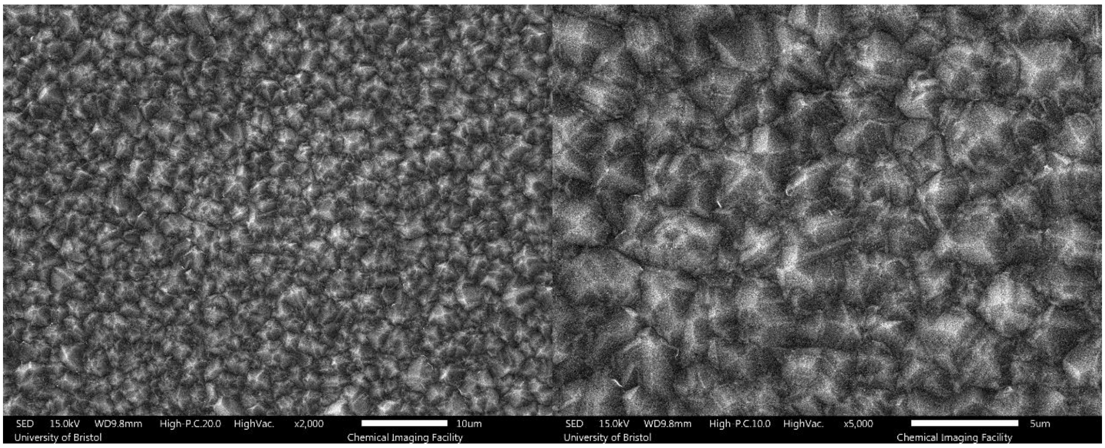

Figure 31: H-BNDD 1 SEM images at left) 2,000x magnification and right) 5,000x magnification

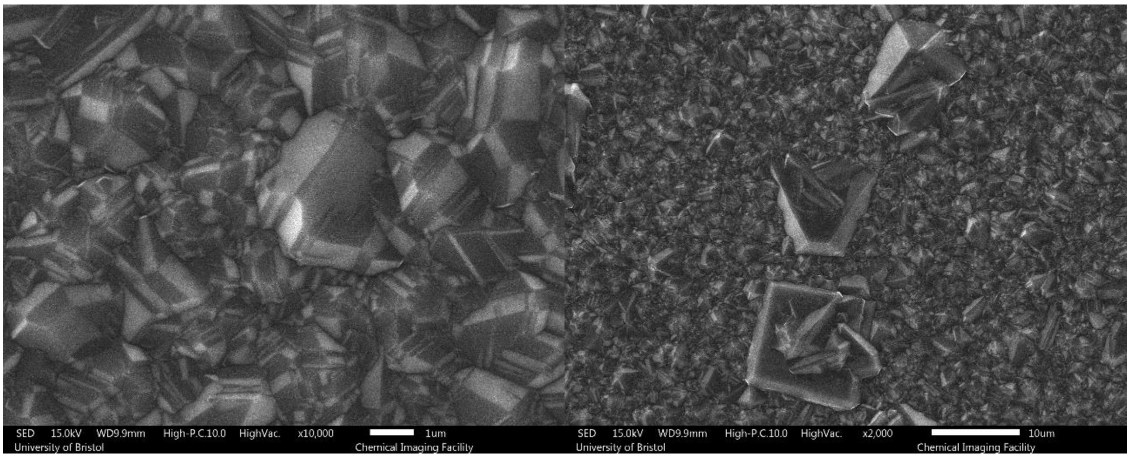

Figure 32: H-BNDD 2 SEM images at left) 10,000 magnification and right) 2,000x magnification

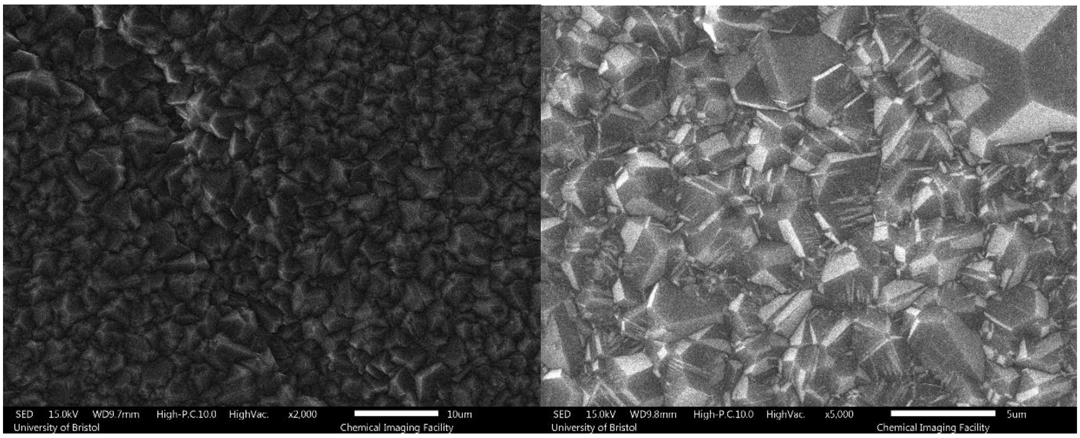

Figure 33: H-BNDD 3 SEM images at left) 2,000x magnification and right) 5,000x magnification

Analysing the different structures of the H-BNDD samples, we can observe facets of <111> and <001> prevalent on the diamond surface. Strikingly, a checkered contrasting pattern can be observed both on a given facets. Comparison with literature using Boron doped samples indicates the checkered patterning observed on the surface is a result of partial graphitisation on the diamond surface as well as boron segregation permeating through the surface layer[104].

In terms of the diamond film quality from the three samples. Extensive production of ledges and terraces can be observed; This is indicative of a high degree of surface roughness, an observation made when performing PEEM analysis on the sample.

Regarding the defect observed on H-BNDD 3, the region in which the defect occurred was analysed by SEM, presenting with a much lower contrast compared to the other samples. This however is only indicative of the defect region, as analysis of other regions of the sample are more characteristic of the other samples secondary electron emission contrast.

3.2.2- Composition

3.2.2.1- X-ray photoemission spectroscopy

XPS utilises x-ray wavelength light to excite electrons within a materials core energy levels. The subsequent quenching of the energy level releases a photon of light in accordance with the photoelectric effect.

$$E_{binding} = E_{Photon} - E_{KE}$$

The re-emitted electron has a different kinetic energy than the incidence, which can be measured by a detector and from that, the bonding energies and composition of the sample can be determined.

XPS is carried out under UHV within the nanoESCA instrument. The XPS parameters are as follows:

The XPS instrument Scienta/Omicron Argus Analyser with a monochromatic Al Ka X-ray source (1486.7eV) was used at a base pressure of 2x10^{-11} mbar. An aperture of A4, pass energy of 50eV was used for survey scans and 20eV for high resolution scans. A -0.5 eV, 0.25s and 0.5s step energy was used for surveys and focused spectra respectively.

Scans were conducted for all H-BNDD samples, as well as the lithium oxide terminated BNDD sample 1 (henceforth known as LiO-BNDD-1). As H-BNDD 1 was the only sample which was terminated with lithium oxide, compositional analysis will focus on this sample only.

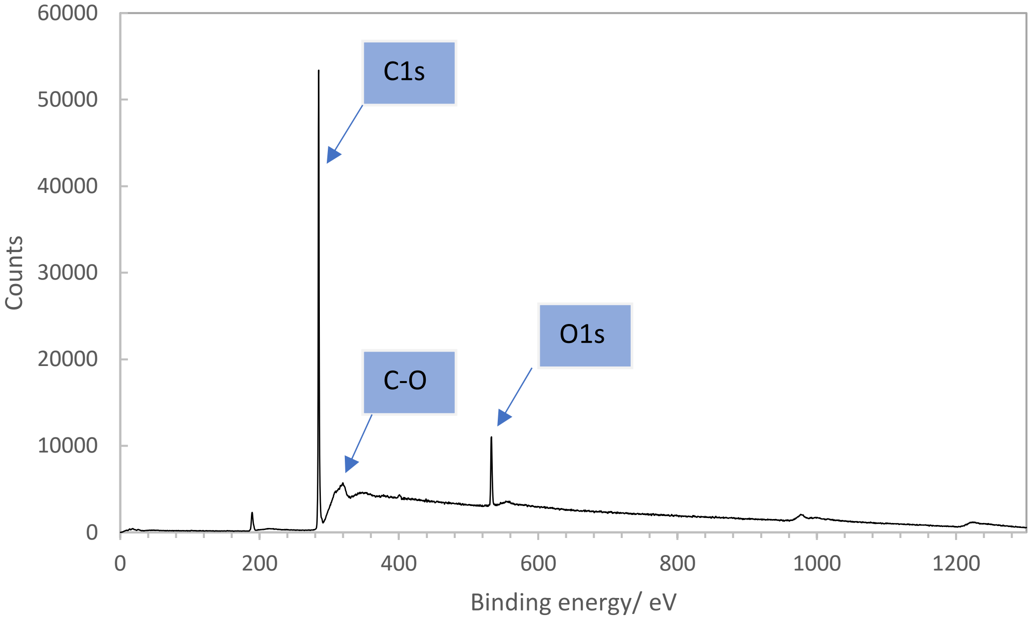

Figure 34: XPS survey of H-BNDD1

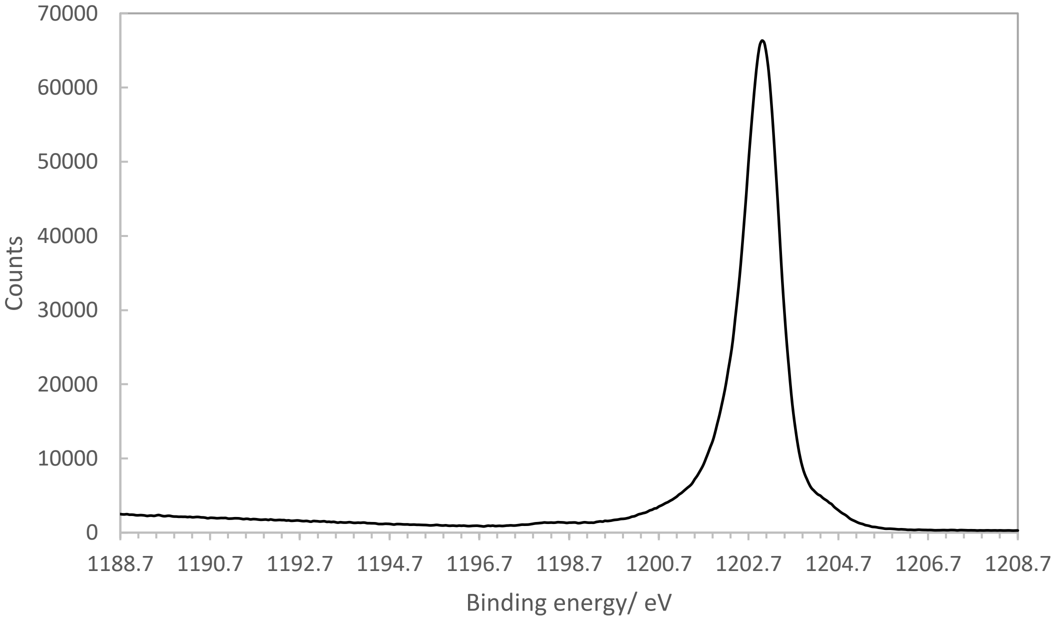

Figure 35: XPS C1s spectra of H-BNDD1

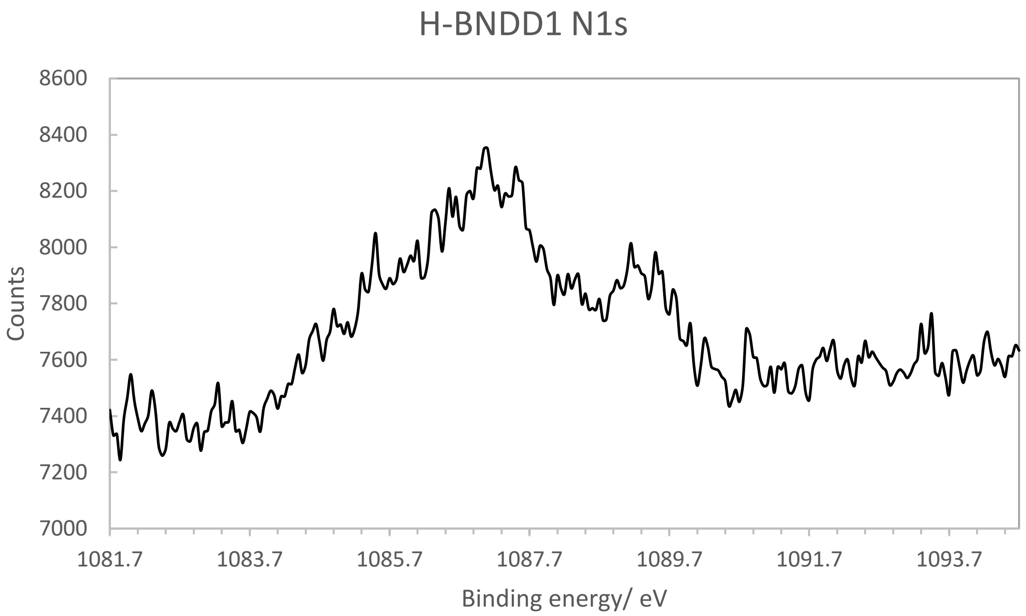

Figure 36: XPS N1s spectra of H-BNDD1

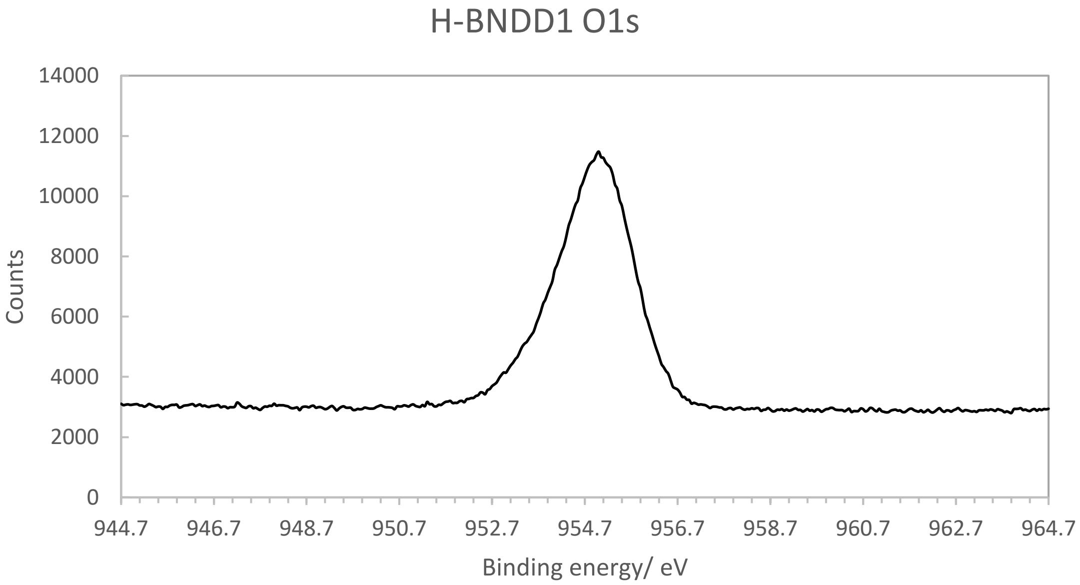

Figure 37: XPS O1s Spectra of H-BNDD1

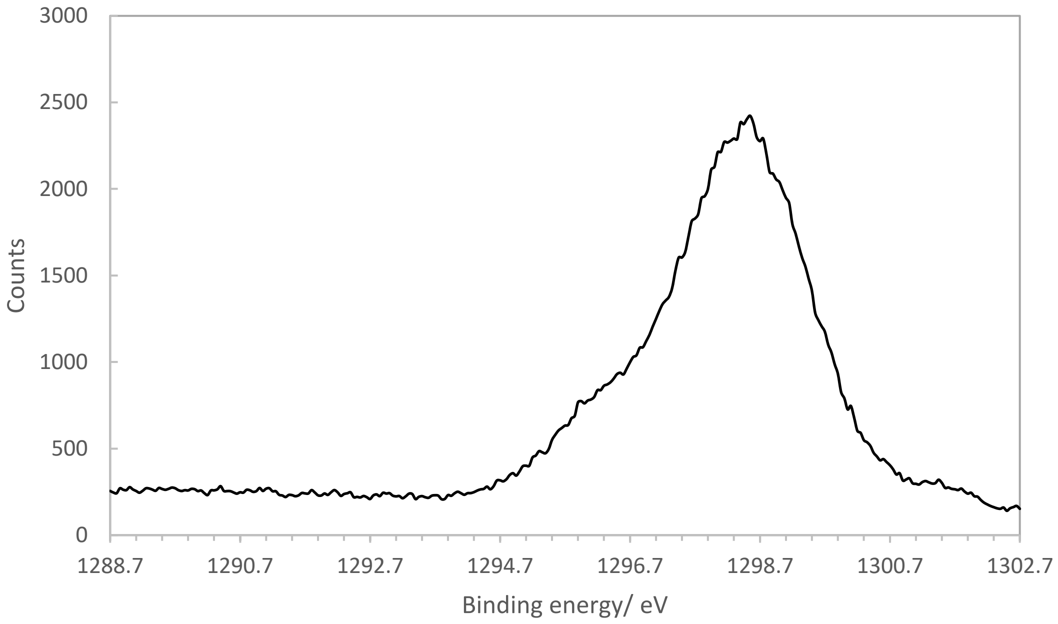

Figure 38: XPS B1s spectra of H-BNDD1

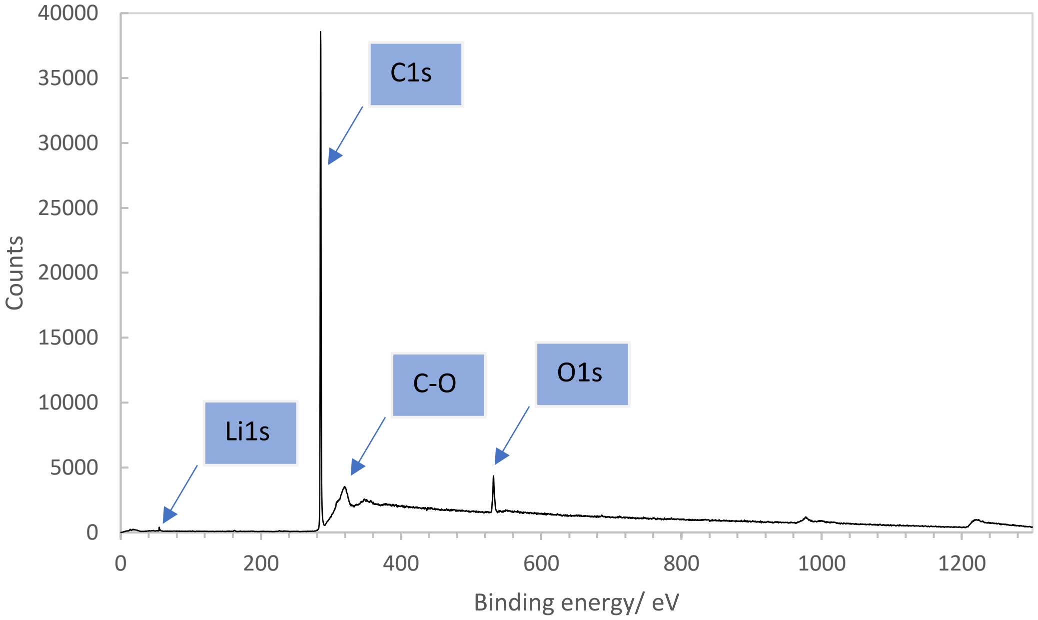

Figure 39: XPS survey of LiO-BNDD1

Observations of H-BNDD 1 spectra indicates the partial presence of boron and oxygen at the surface of the diamond material. The boron presence could indicate migration of the dopant species closer to the diamond surface, whilst the oxygen presence is likely from air exposure. The characteristic carbon 1s peak at an intensity several magnitudes greater than other species such as oxygen. With regards to oxygen, it’s 1s and carbon attenuation peak before deposition of lithium is larger than after the deposition of lithium onto the surface, this could indicate potential removal of oxygen from

BNDD diamond from either the deposition process or the annealing steps that were taking prior to analysis. As a larger proportion of oxygen was expected from the latter spectra, this could indicate ineffective surface adhesion to the co-doped diamond film.

With regards to the lithium peak on the LiO-BNDD spectra, the relative sensitivity of lithium with regards to carbon is 0.0568, thus the peak only shows as a pixel on the far left of the spectra. Despite this, the question remains on whether the amount of lithium terminated onto the surface is characteristic of a full metal layer, half metal layer or lesser adhesion to the surface. Research of relevant literature gives no explanation for these findings.

3.2.3- Work function and emission

3.2.3.1- Ultraviolet photoelectron spectroscopy

Like XPS, UPS employs an energy source to excite the electrons within the materials structure, which are then re-emitted to a detector. The employment of UV light in place of X-rays permits the probing of valence band electrons from a materials surface. The resulting spectra produced provides an indication on the electronic structure of the diamond film's surface.

From binding energy range 0 to 12, we can deduce the valence band minima of our material's surface, as well as a general indication of the band structure. For binding energy range 15 onwards, we can determine the secondary electron peak, the high energy cut off point for our material, and most notably, the work function.

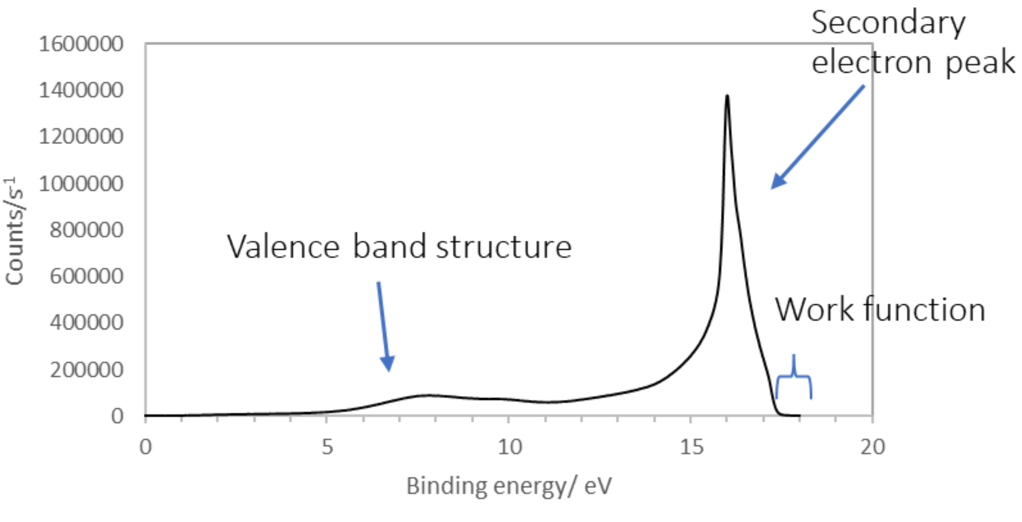

Figure 40: Illustration of the electronic structures within UPS spectra

H-BNDD 1 and LiO-BNDD 1 were both analysed via this method. The UPS instrumentation setup is as follows: UPS measurements were taken using Focus/ScientaOmicron NanoESCA II with monochromatic He I source (21.2eV). The focus of the instrumentation had a field of view of (243.12um), a pass energy of (50eV), slit width of (0.5mm) with a contrast aperture inserted in the back of the focal plane.

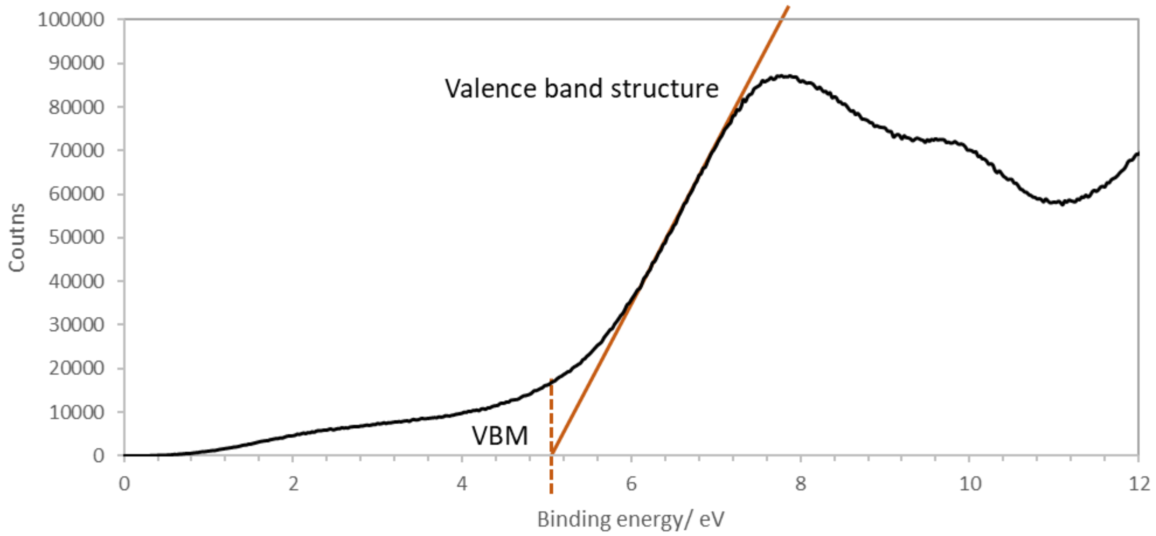

Figure 41: Valence band structure from H-BNDD UPS spectra

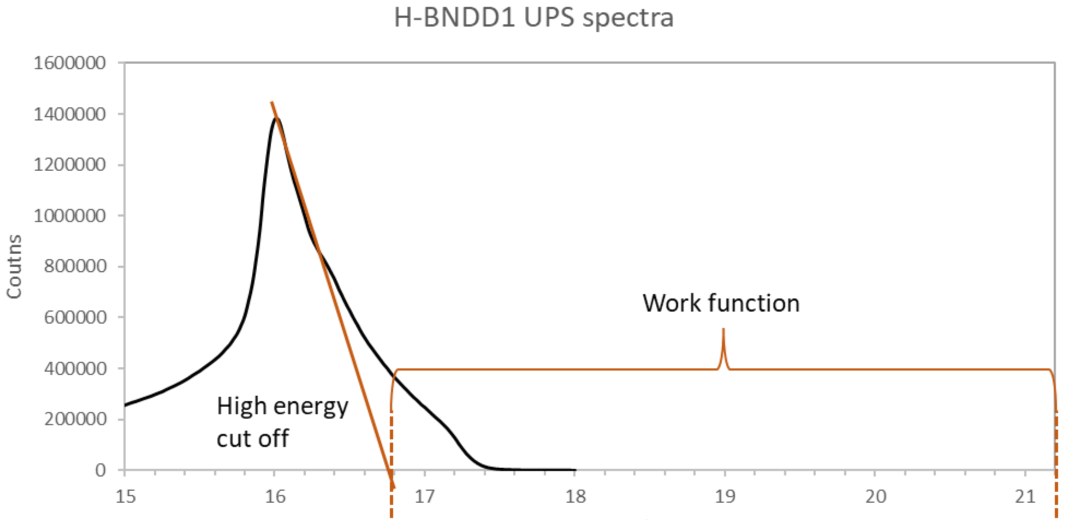

Figure 42: high energy cut off and work function structures from H-BNDD UPS spectra

UPS spectra of H-BNDD1 indicates a VBM of ~4.48eV from the fermi energy of the sample. The high energy cut off was determined as 16.8 eV and with this and the helium UV source energy of 21.2eV, we can determine the work function for our H-terminated material to be 4.4eV. This work function is like that observed by C.I. Pakes *et. al.* where they determined the work function of annealed hydrogen terminated diamond to be ~4.37eV.

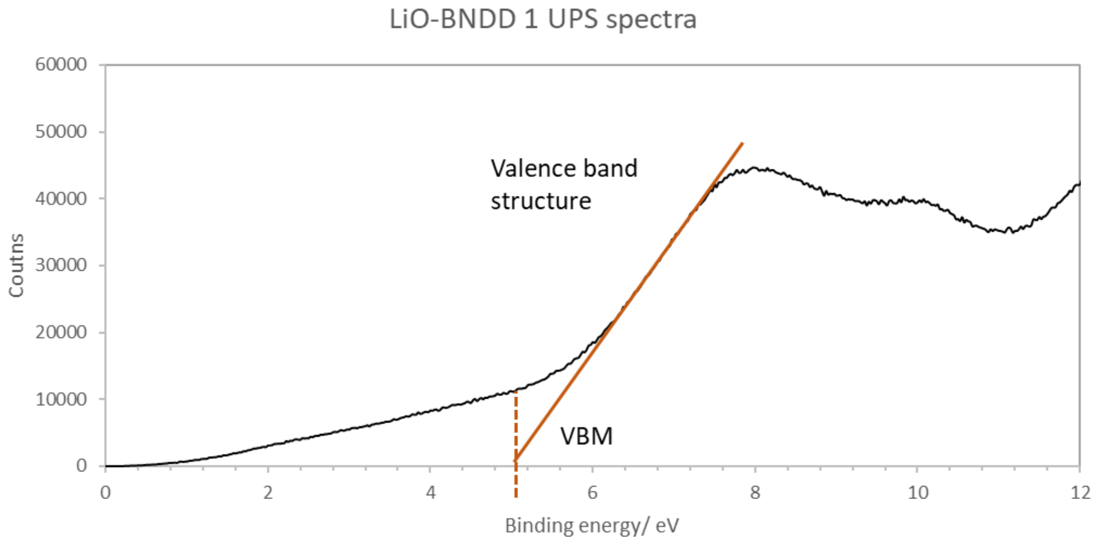

Figure 43: Valence band structure from LiO-BNDD UPS spectra

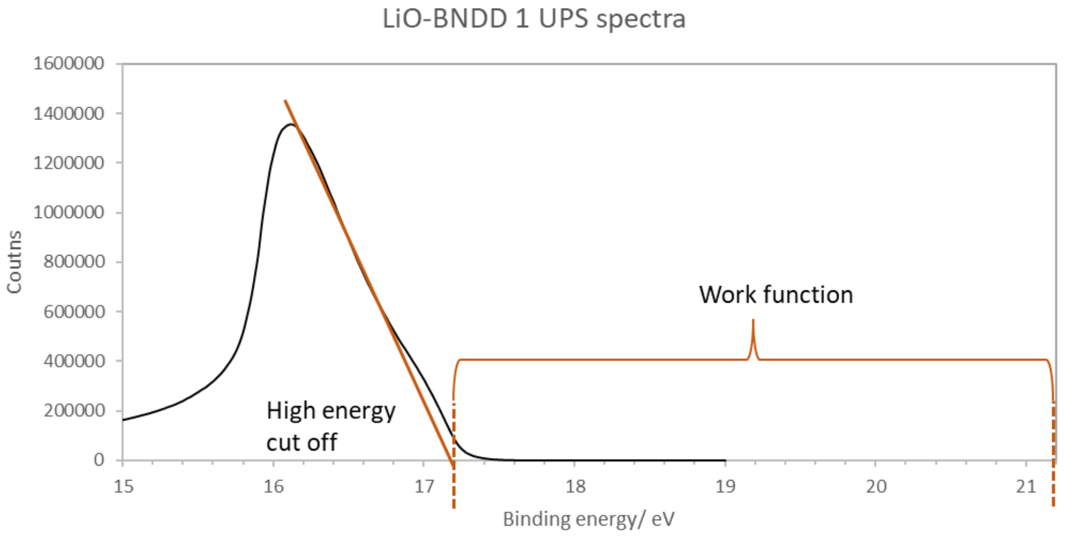

Figure 44: high energy cut off and work function structures from LiO-BNDD UPS spectra

For LiO-BNDD sample, we can determine the VBM of the surface is ~4.53eV, with the high energy cut-off of the sample being 17.2. With a work function of 4eV, we can conclude that, assuming the region measured had lithium oxide terminations present, that the addition of such a surface termination reduces the work function of BNDD diamond by 0.37eV.

3.2.3.2- Photoemission electron spectroscopy

PEEM used the same instrumentation as UPS. The different between the two is that PEEM can produce a spectra from individual states within a chosen area of a sample which, when processed, and provide crucial work function data based on a topological region of the sample. This can both give indications as the distribution of the work function across a grown diamond surface, as well as provide insight into the surface roughness of the sample.

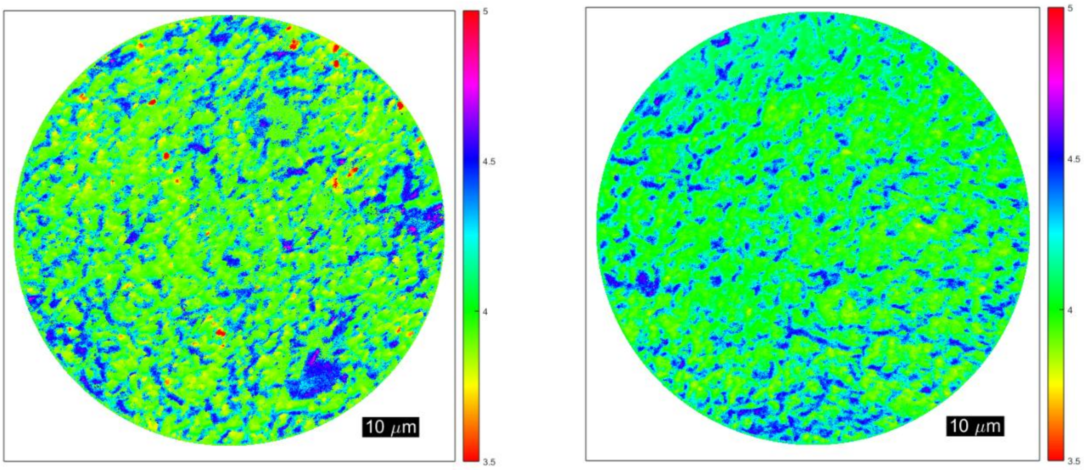

Figure 45: Work function plots for left) H-BNDD, right) LiO-BNDD

When comparing both samples to their UPS spectra's, we can validate that the estimated work function determined prior is consistent with the heat map of both our samples. When comparing the two heat maps, we can see that, like the calculated work function, there is only minor differences in the topology of these work functions map. From first glance, we can determine that the greater prevalence of blue regions on H-BNDD likely resultant of the samples higher work function. Furthermore, the fluctuation in colour can be indicative of a very rough surface, which is of detriment to the work function of the sample. For LiO-BNDD, a greater uniformity can be identified across the sample surface, this likely resultant of the annealing process causing surface reconstruction, subsequently improving work function of the sample.

With these heat maps, surface roughness can be quantitatively analysed. By grey scaling the work function map, employing MATLAB allows for a population distribution to be produced.

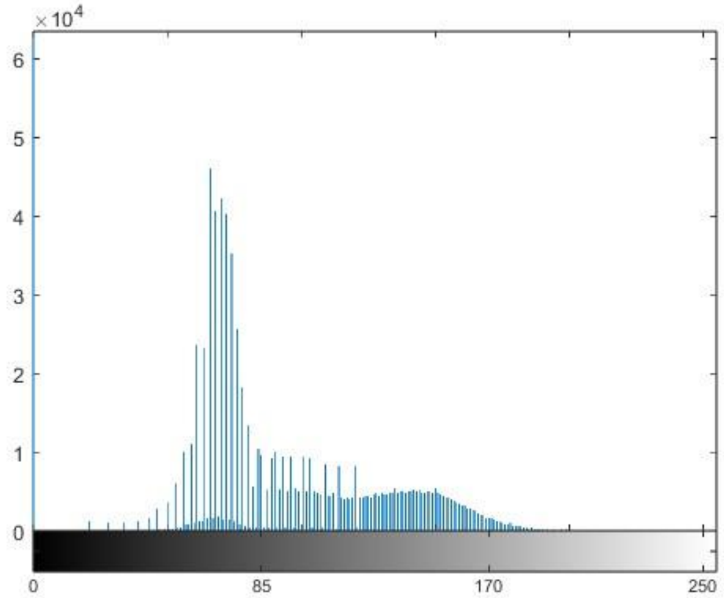

Figure 46: Distribution plot of greyscale work function map H-BNDD

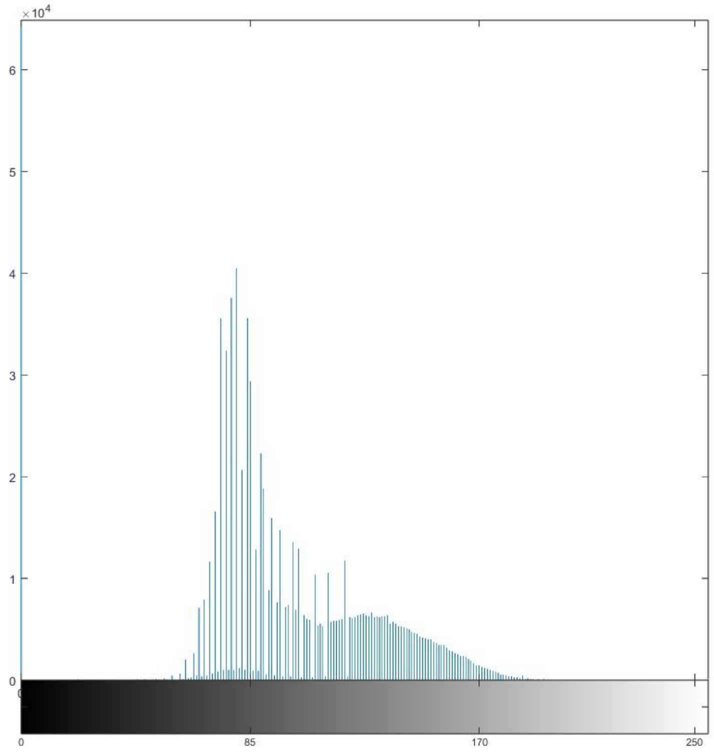

Figure 46: Distribution plot of greyscale work function map H-BNDD

The histogram for each sample gives us a clearer picture as to the distribution of work function across each surface. For the x axis, each tick increase of 85 equates to 0.5 eV in terms of work function, starting form 3.5eV. Surprisingly, examination of the region of lower value work function shows that the H-BNDD sample presents with a small population of low work function regions on the diamond surface. This, however, is couples with a much larger distribution of work functions across the histogram. This difference in density of distribution likely accounts for the larger work function seen in H-BNDD

4- Discussion & conclusion

4.1- Results overview

Several samples of boron and nitrogen doped diamond films were synthesised and characterised for their work function values and growth quality. The samples were grown using MPCVD on a molybdenum substrate. Though identical conditions were used for each film growth, the surface quality of one of the samples varied drastically, likely due to prominence of graphitised surface defects. It was observed that the co doping film under SEM, gave rise to highly disordered surface morphology which likely resulted in negative implications for the work function calculations later tested, as well as the potential adhesion of the terminating species to the diamond substrate. BNDD sample 1 was selected and compared between its hydrogen terminated and lithium oxide terminated forms. Subsequent compositional analysis of the sample at both stages indicated both the removal of oxygen from the diamond surface after ozone treatment, as well as potential inefficient binding of lithium to the oxidised surface. Despite this, we were able to present the reduction from a work function of 4.37eV for the hydrogen terminated sample, to 4eV for the lithium oxide terminated sample. Comparatively, these work function results are much larger in value compared to research literature for different dopant systems.[77]

While positive results were recorded, the lack of the repeatability within the study means that reproduction of work is necessary to validate the results published.

4.2- Future work

The primary intention of this study was to characterise the emission current of the diamond growth via use of the thermionic emission current simulator (TECsim), an apparatus used to raise the temperature of the sample and measure the density of electron emitted from the sample surface. Due to down time of the equipment, along with time constrains following the repair of the apparatus, no usable data was collected from using the machine.

It would be imperative to study the samples produced for this study in an applicable environment like that of the TECsim, as though the work functions calculated can give an indication as the threshold temperature needed for thermionic emission from a given sample, the functional use of the TECsim allows for the quantitative reporting of the emissions produced from such an emitter at a given temperature. Furthermore, the stability of the diamond film can be deduced by utilisation of the TECsim, as desorption of the termination species from the diamond surface would indicate what temperatures the device is operable to.

The initial scope of the project included a variety of diamond film growths which would have proved beneficial for supporting the results attained from this study. A key developmental scope was the production of a n-p junction rather than the gradient like growth of the samples used for this study. Furthermore, an additional metal (lithium or magnesium) oxide layer was to be added to the diamond surface, with the rationale that additional termination layers on the diamond surface could further drive the reduction in work function.

References

(1) Zhang, Y.; Yin, Q. Z. Carbon and other light element contents in the Earth's core based on first-principles molecular dynamics. *Proc Natl Acad Sci U S A* 2012, *109* (48), 19579-19583. DOI: 10.1073/pnas.1203826109 From NLM.

(2) Allègre, C. J.; Poirier, J.-P.; Humler, E.; Hofmann, A. W. The chemical composition of the Earth. *Earth and Planetary Science Letters* 1995, *134* (3), 515-526. DOI: https://doi.org/10.1016/0012-821X(95)00123-T.

(3) Eatemadi, A.; Daraee, H.; Karimkhanloo, H.; Kouhi, M.; Zarghami, N.; Akbarzadeh, A.; Abasi, M.; Hanifehpour, Y.; Joo, S. W. Carbon nanotubes: properties, synthesis, purification, and medical applications. *Nanoscale Res Lett* 2014, *9* (1), 393. DOI: 10.1186/1556-276x-9-393 From NLM.

(4) Rathinavel, S.; Priyadharshini, K.; Panda, D. A review on carbon nanotube: An overview of synthesis, properties, functionalization, characterization, and the application. *Materials Science and Engineering: B* 2021, *268*, 115095. DOI: https://doi.org/10.1016/j.mseb.2021.115095.

(5) Mohan, M.; Sharma, V. K.; Kumar, E. A.; Gayathri, V. Hydrogen storage in carbon materials—A review. *Energy Storage* 2019, *1* (2), e35. DOI: https://doi.org/10.1002/est2.35.

(6) Andel. Eight allotropes of carbon. In.*SVG*, 2 ed.; carbon, E. a. o., Ed.; Wikipedia: Wikipedia, 2019; Vol. 512x512, p carbon allotropes.

(7) Donaldson, L. Graphene: invisible to water: Carbon. *Materials Today* 2012, *15* (3), 82. DOI: https://doi.org/10.1016/S1369-7021(12)70037-8.

(8) parker, S. Ranked: The World's Top Diamond Mining Countries, by Carats and Value. In *Visualcapitalist*, 1 ed.; Visualcapitalist: Visualcapitalist.com, 2023; p 1.

(9) Shirey, S. B.; Shigley, J. E. RECENT ADVANCES IN UNDERSTANDING THE GEOLOGY OF DIAMONDS. *Gems & Gemology* 2013, *49* (4).

(10) Gernon, T. M.; Jones, S. M.; Brune, S.; Hincks, T. K.; Palmer, M. R.; Schumacher, J. C.; Primiceri, R. M.; Field, M.; Griffin, W. L.; O'Reilly, S. Y.; et al. Rift-induced disruption of cratonic keels drives kimberlite volcanism. *Nature* 2023, *620* (7973), 344-350. DOI: 10.1038/s41586-023-06193-3.

(11) survey, K. g. What are kimberlites. 2000.

(12) Nimis, P. Pressure and Temperature Data for Diamonds. *Reviews in Mineralogy and Geochemistry* 2022, *88* (1), 533-565. DOI: 10.2138/rmg.2022.88.10 (acccessed 4/10/2024).

(13) Lylie. *The true cost of mined diamonds*. Lylie, 2017. https://lylies.com/pages/true-cost-of-a-diamond (accessed 2023 13 October).

(14) RockHer. *How diamonds are mined*. https://www.rockher.com/pages/how-diamonds-are-mined (accessed 2024 13 Novemebr 2023).

(15) Zhdanov, V.; Smirnov, P.; Andrzejewski, L.; Bondareva, J.; Evlashin, S. Comparative analysis of labor input required to produce one carat at different methods of synthesis and mining of diamonds. *Heliyon* 2022, *8* (11), e11519. DOI: 10.1016/j.heliyon.2022.e11519 From NLM.

(16) Mamonov, S.; Triantoro, T. Subjectivity of Diamond Prices in Online Retail: Insights from a Data Mining Study. *Journal of Theoretical and Applied Electronic Commerce Research* 2018, *13* (2), 15-28.

(17) Askeland, D. R. Example 3-15: determining the packing factor for diamond cubic silicon. In *The Science and Engineering of Materials*, Vol. 82; Cengage, 2006.

(18) Ellis, A. *Taching general chemistry: a materials science companion (3rd ed.)*; American chemical society, 1995.

(19) Zulkharnay, R. Electron Emission Studies of Scandium

on Diamond for Thermionic Solar

Energy Generation Devices. University of brisotl, open access, 2023. https://research-information.bris.ac.uk/ws/portalfiles/portal/369226352/Final_Copy_2023_06_20_Zulkharnay_R_PhD.pdf.

(20) Wen, B.; Zhao, J.; Bucknum, M. J.; Yao, P.; Li, T. First-principles studies of diamond polytypes. *Diamond and Related Materials* 2008, *17* (3), 356-364. DOI: https://doi.org/10.1016/j.diamond.2008.01.020.

(21) *Space group diagrams and tables*. Birbeck college, university of london, 1997-1999. http://img.chem.ucl.ac.uk/sgp/large/227bz1.htm (accessed 2023 20 October).

(22) Sushko, G. Atomistic molecular dynamics approach for channeling of charged particles in oriented crystals. 2015.

(23) Weber, M. J. *Handbook of optical materials*; The CRC press, 2000.

(24) Spear, K. E. *Synthetic Diamond: Emerging CVD Science and Technology*; John wiley and sons, 1994, 1994.

(25) Yamada, H. 10 - Diamond. In *Single Crystals of Electronic Materials*, Fornari, R. Ed.; Woodhead Publishing, 2019; pp 331-350.

(26) Prelas. *Handbook of industrial diamonds*; CRC press, 1998.

(27) Makino, T.; Kato, H.; Ogura, M.; Watanabe, H.; Ri, S.-G.; Chen, Y.; Yamasaki, S.; Okushi, H. Electrical and optical characterizations of (001)-oriented homoepitaxial diamond p–n junction. *Diamond and Related Materials* 2006, *15*, 513-516. DOI: 10.1016/j.diamond.2005.11.021.

(28) Ito, T.; Watanabe, T.; Irie, M.; Nakamura, J.; Teraji, T. Electron emissions from CVD diamond surfaces. *Diamond and Related Materials* 2003, *12* (3), 434-441. DOI: https://doi.org/10.1016/S0925-9635(03)00069-4.

(29) savage, N. Quantum diamond sensors. *Nature* 2021, *591*. DOI: https://doi.org/10.1038/d41586-021-00742-4.

(30) Pinault, M. A.; Barjon, J.; Kociniewski, T.; Jomard, F.; Chevallier, J. The n-type doping of diamond: Present status and pending questions. *Physica B: Condensed Matter* 2007, *401-402*, 51-56. DOI: https://doi.org/10.1016/j.physb.2007.08.112.

(31) Hyperphysics. Fermi level and fermi function. Georgia state university: Hyperphysics, 2020.

(32) Hyperphysics. Doped semiconductors. Georgia state univesity: Hyperphysics, 2020.

(33) Jensen, C.; Aaserud, F.; Kragh, H.; Rüdinger, E.; Stuewer, R. H. Prelude: Beta-Spectrum Research in the Pre-Nuclear Years, 1900–1911. In *Controversy and Consensus: Nuclear Beta Decay 1911–1934*, Jensen, C., Aaserud, F., Kragh, H., Rüdinger, E., Stuewer, R. H. Eds.; Birkhäuser Basel, 2000; pp 1-28.

(34) Donald Blaufox, M. Becquerel and the discovery of radioactivity: Early concepts. *Seminars in Nuclear Medicine* 1996, *26* (3), 145-154. DOI: https://doi.org/10.1016/S0001-2998(96)80019-5.

(35) McCarthy, P. T.; Reifenberger, R. G.; Fisher, T. S. Thermionic and Photo-Excited Electron Emission for Energy-Conversion Processes. *Frontiers in Energy Research* 2014, *2*, Review. DOI: 10.3389/fenrg.2014.00054.

(36) Kiziroglou, M. E.; Li, X.; Zhukov, A. A.; de Groot, P. A. J.; de Groot, C. H. Thermionic field emission at electrodeposited Ni–Si Schottky barriers. *Solid-State Electronics* 2008, *52* (7), 1032-1038. DOI: https://doi.org/10.1016/j.sse.2008.03.002.

(37) Chiu, F.-C. A Review on Conduction Mechanisms in Dielectric Films. *Advances in Materials Science and Engineering* 2014, *2014*, 578168. DOI: 10.1155/2014/578168.

(38) Rahman, E.; Nojeh, A. Semiconductor thermionics for next generation solar cells: photon enhanced or pure thermionic? *Nature Communications* 2021, *12* (1), 4622. DOI: 10.1038/s41467-021-24891-2.

(39) Richardson, O. W. Physics 1928. In *Physics 1922–1941*, Elsevier, 2013; pp 219-238.

(40) Rymer, T. B.; Richardson, O. W. The emission of positive ions by platinum when heated oxygen. *Proceedings of the Royal Society of London. Series A - Mathematical and Physical Sciences* 1936, *153* (879), 422-442. DOI: doi:10.1098/rspa.1936.0012.

(41) Wehnelt, A. Über den Austritt negativer Ionen aus glühenden Metallverbindungen und damit zusammenhängende Erscheinungen. *Annalen der Physik* 1904, *319* (8), 425-468. DOI: https://doi.org/10.1002/andp.19043190802.

(42) Richardson, O. W. The Emission of Electrons from Tungsten at High Temperatures: An Experimental Proof That the Electric Current in Metals Is Carried by Electrons. *Science* 1913, *38* (967), 57-61. DOI: doi:10.1126/science.38.967.57.

(43) Compton, K. T.; Richardson, O. W. XLV. The photoelectric effect.—II. *The London, Edinburgh, and Dublin Philosophical Magazine and Journal of Science* 1913, *26* (154), 549-567. DOI: 10.1080/14786441308635002.

(44) James, M. C.; Fogarty, F.; Zulkharnay, R.; Fox, N. A.; May, P. W. A review of surface functionalisation of diamond for thermionic emission applications. *Carbon* 2021, *171*, 532-550. DOI: https://doi.org/10.1016/j.carbon.2020.09.019.

(45) Go, D.; Haase, J.; George, J.; Mannhart, J.; Wanke, R.; Nojeh, A.; Nemanich, R. Thermionic Energy Conversion in the Twenty-first Century: Advances and Opportunities for Space and Terrestrial Applications. *Frontiers in Mechanical Engineering* 2017, *3*, 13. DOI: 10.3389/fmech.2017.00013.

(46) Campbell, M. F.; Celenza, T. J.; Schmitt, F.; Schwede, J. W.; Bargatin, I. Progress Toward High Power Output in Thermionic Energy Converters. *Advanced Science* 2021, *8* (9), 2003812. DOI: https://doi.org/10.1002/advs.202003812.

(47) Chen, W. Introduction to thermal atomic batteries. Stanford university: Stanford University, 2011; p 1.

(48) Hatsopoulos, G. N.; Gyftopoulos, E. P. *Thermionic energy conversion. Volume II. Theory, technology, and application*; MIT Press,Cambridge, MA, 1979.

(49) Child, C. D. Discharge From Hot CaO. *Physical Review (Series I)* 1911, *32* (5), 492-511. DOI: 10.1103/PhysRevSeriesI.32.492.

(50) Moyzhes, B. Y.; Geballe, T. H. The thermionic energy converter as a topping cycle for more efficient heat engines—new triode designs with a longitudinal magnetic field. *Journal of Physics D: Applied Physics* 2005, *38* (5), 782. DOI: 10.1088/0022-3727/38/5/017.

(51) Wanke, R.; Hassink, G. W. J.; Stephanos, C.; Rastegar, I.; Braun, W.; Mannhart, J. Magnetic-field-free thermoelectronic power conversion based on graphene and related two-dimensional materials. *Journal of Applied Physics* 2016, *119* (24). DOI: 10.1063/1.4955073 (acccessed 4/10/2024).

(52) Liebermann, R. C. Multi-anvil, high pressure apparatus: a half-century of development and progress. *High Pressure Research* 2011, *31* (4), 493-532. DOI: 10.1080/08957959.2011.618698.

(53) Palyanov, Y. N.; Borzdov, Y. M.; Kupriyanov, I. N.; Khohkhryakov, A. F.; Nechaev, D. V. Rare-earth metal catalysts for high-pressure synthesis of rare diamonds. *Scientific Reports* 2021, *11* (1), 8421. DOI: 10.1038/s41598-021-88038-5.

(54) Sumiya, H.; Toda, N.; Satoh, S. Development of high-quality large-size synthetic diamond crystals. *SEI Technical Review* 2005, 10-16.

(55) Yin, L.-W.; Li, M.-S.; Cui, J.-J.; Zou, Z.-D.; Liu, P.; Hao, Z.-Y. Diamond formation using Fe3C as a carbon source at high temperature and high pressure. *Journal of Crystal Growth* 2002, *234* (1), 1-4. DOI: https://doi.org/10.1016/S0022-0248(01)01677-3.

(56) Angus, J. C.; Will, H. A.; Stanko, W. S. Growth of Diamond Seed Crystals by Vapor Deposition. *Journal of Applied Physics* 1968, *39* (6), 2915-2922. DOI: 10.1063/1.1656693 (acccessed 4/10/2024).

(57) Deryagin, B. V.; Fedoseev, D. V. Epitaxial Synthesis of Diamond in the Metastable Region. *Russian Chemical Reviews* 1970, *39* (9), 783. DOI: 10.1070/RC1970v039n09ABEH002022.

(58) Khachatryan, A. K.; Aloyan, S. G.; May, P. W.; Sargsyan, R.; Khachatryan, V. A.; Baghdasaryan, V. S. Graphite-to-diamond transformation induced by ultrasound cavitation. *Diamond and Related Materials* 2008, *17* (6), 931-936. DOI: https://doi.org/10.1016/j.diamond.2008.01.112.

(59) Bellardita, M.; Di Paola, A.; Yurdakal, S.; Palmisano, L. Preparation of Catalysts and Photocatalysts Used for Similar Processes. 2019; pp 25-56.

(60) Eaton-Magana, S. RECENT ADVANCES IN CVD SYNTHETIC DIAMOND QUALITY. Gems and gemology, 2012; p 4.

(61) halliwell, S. Investigations into the plasma formed by a

microwave reactor used for the chemical vapour

deposition of diamond. University of bristol, University of bristol, 2012.

(62) Tsang, R. S. CHARACTERISATION OF THE GAS-PHASE ENVIRONMENT IN A HOT FILAMENT DIAMOND CHEMICAL VAPOUR DEPOSITION CHAMBER USING MOLECULAR BEAM MASS SPECTROMETRY. Univeristy of bristol: 1997.

(63) Ma, Y.; Chen, J.; Wang, C. Growth of Diamond Thin Film and Creation of NV Centers. 2022.

(64) Chang, C.; Liao, Y.; Wang, G. Z.; Ma, Y. R.; Fang, R. C. 4 - CVD Diamond Growth. In *Crystal Growth Technology*, Byrappa, K., Ohachi, T., Michaeli, W., Warlimont, H., Weber, E. Eds.; William Andrew Publishing, 2003; pp 93-141.

(65) Sergeichev, K. F.; Lukina, N. A.; Bolshakov, A. P.; Ralchenko, V. G.; Arutyunyan, N. R.; Vlasov, I. I. Polycrystal diamond growth in a microwave plasma torch. *Plasma Physics Reports* 2010, *36* (13), 1272-1277. DOI: 10.1134/S1063780X10130301.

(66) Borrell, A.; Salvador, M. Advanced Ceramic Materials Sintered by Microwave Technology. 2018.

(67) Impedance matching.

(68) Locher, R.; Wagner, J.; Fuchs, F.; Maier, M.; Gonon, P.; Koidl, P. Optical and electrical characterization of boron-doped diamond films. *Diamond and Related Materials* 1995, *4* (5), 678-683. DOI: https://doi.org/10.1016/0925-9635(94)05297-2.

(69) Maeda, H.; Ohtsubo, K.; Kameta, M.; Saito, T.; Kusakabe, K.; Morooka, S.; Asano, T. Growth behavior of boron-doped diamond in microwave plasma-assisted chemical vapor deposition using trimethylboron as the dopant source. *Diamond and Related Materials* 1998, *7* (1), 88-95. DOI: https://doi.org/10.1016/S0925-9635(98)80001-0.

(70) Issaoui, R.; Achard, J.; Silva, F.; Tallaire, A.; Tardieu, A.; Gicquel, A.; Pinault, M. A.; Jomard, F. Growth of thick heavily boron-doped diamond single crystals: Effect of microwave power density. *Applied Physics Letters* 2010, *97* (18). DOI: 10.1063/1.3511449 (acccessed 4/10/2024).

(71) Li, Y.; Dai, B.; Ralchenko, V. G.; Lyu, J.; Hao, X.; Zhao, J.; Zhang, S.; Liu, K.; Han, J.; Bolshakov, A. P.; et al. Growth of single-crystal diamond by microwave plasma CVD with high precursor utilization using cyclic gas injection and control of carbonaceous species content with optical emission spectroscopy. *Vacuum* 2022, *206*, 111529. DOI: https://doi.org/10.1016/j.vacuum.2022.111529.

(72) Chen, K.; Tao, T.; Hu, W.; Ye, Y.; Zheng, K.; Ye, J.; Zhi, T.; Wang, X.; Liu, B.; Zhang, R. High-speed growth of high-quality polycrystalline diamond films by MPCVD. *Carbon Letters* 2023, *33* (7), 2003-2010. DOI: 10.1007/s42823-023-00534-y.

(73) Yang, D.; Guo, L.; Wang, B.; Jin, S.; Zhu, J.; Zhai, M. Hydrogen plasma characteristics in a microwave chemical vapor deposition chamber. *Materials Science and Engineering: B* 2023, *292*, 116422. DOI: https://doi.org/10.1016/j.mseb.2023.116422.

(74) Sabat, K. C.; Rajput, P.; Paramguru, R. K.; Bhoi, B.; Mishra, B. K. Reduction of Oxide Minerals by Hydrogen Plasma: An Overview. *Plasma Chemistry and Plasma Processing* 2014, *34* (1), 1-23. DOI: 10.1007/s11090-013-9484-2.

(75) Jiang, H.; Liu, F.; Yan, H.; Si, L.; Dou, Z. Etching effects of hydrogen plasma treatment on diamond surfaces. *Surface and Coatings Technology* 2019, *363*, 12-17. DOI: https://doi.org/10.1016/j.surfcoat.2019.02.007.

(76) *CVD diamond handbook*. De Beers group, https://e6cvd.com/media/wysiwyg/pdf/CVD_Diamond_Handbook_digital_01.07.20.pdf (accessed 2023 december 2023).

(77) holmes, R.-D. Nitrogen-Doped Diamond; A Thermionic

Investigation on the Effects of Lithium

Oxide Termination. Univeristy of bristol, University of bristol, 2023.

(78) root, A. Boron and nitrogen in diamond: an

ab initio simulation, plasma emission

spectroscopy and material deposition &

characterisation study. UNIVERSITY OF BRISTOL, UNIVERSITY OF BRISTOL, 2018.

(79) Fujimori, N.; Imai, T.; Doi, A. Characterization of conducting diamond films. *Vacuum* 1986, *36* (1), 99-102. DOI: https://doi.org/10.1016/0042-207X(86)90279-4.

(80) Ngambou, M. W. N.; Pellet-Mary, C.; Brinza, O.; Antonino, A.; Hetet, G.; Tallaire, A.; Bénédic, F.; Achard, J. Improving NV centre density during diamond growth by CVD process using N2O gas. *Diamond and Related Materials* 2022, *123*, 108884. DOI: https://doi.org/10.1016/j.diamond.2022.108884.

(81) Lambert, N.; Weiss, Z.; Klimša, L.; Kopeček, J.; Gedeonová, Z.; Hubík, P.; Mortet, V. Highly phosphorus-doped polycrystalline diamond growth and properties. *Diamond and Related Materials* 2022, *125*, 108964. DOI: 10.1016/j.diamond.2022.108964.

(82) Yu, S.; Xu, J.; Kato, H.; Yang, N.; Schulte, A.; Schönherr, H.; Jiang, X. Phosphorus-Doped Nanocrystalline Diamond for Supercapacitor Application. *ChemElectroChem* 2019, *6* (4), 1088-1093. DOI: https://doi.org/10.1002/celc.201801543.

(83) Schwander, M.; Partes, K. A review of diamond synthesis by CVD processes. *Diamond and Related Materials* 2011, *20* (9), 1287-1301. DOI: https://doi.org/10.1016/j.diamond.2011.08.005.

(84) Brinza, O.; Achard, J.; Silva, F.; Bonnin, X.; Barroy, P.; Corte, K. D.; Gicquel, A. Dependence of CVD diamond growth rate on substrate orientation as a function of process parameters in the high

microwave power density regime. *physica status solidi (a)* 2008, *205* (9), 2114-2120. DOI: https://doi.org/10.1002/pssa.200879716.

(85) Atakan, B.; Lummer, K.; Kohse-Höinghaus, K. Diamond deposition in acetylene–oxygen flames: nucleation and early growth on molybdenum substrates for different pretreatment procedures. *Physical Chemistry Chemical Physics* 1999, *1* (13), 3151-3156, 10.1039/A901945F. DOI: 10.1039/A901945F.

(86) Riley, P. R.; Joshi, P.; Narayan, J.; Narayan, R. J. Enhanced nucleation and large-scale growth of CVD diamond via surface-modification of silicon-incorporated diamond-like carbon thin films. *Diamond and Related Materials* 2021, *120*, 108630. DOI: https://doi.org/10.1016/j.diamond.2021.108630.

(87) Fox, O. J. L.; Holloway, J. O. P.; Fuge, G. M.; May, P. W.; Ashfold, M. N. R. Electrospray Deposition of Diamond Nanoparticle Nucleation Layers for Subsequent CVD Diamond Growth. *MRS Proceedings* 2009, *1203*, 1203-J1217-1227. DOI: 10.1557/PROC-1203-J17-27 From Cambridge University Press Cambridge Core.

(88) Rased, N. H.; Vengadaesvaran, B.; Raihan, S. R. S.; Rahim, N. A. Chapter 6 - Introduction to solar energy and its conversion into electrical energy by using dye-sensitized solar cells. In *Energy Materials*, Dhoble, S. J., Kalyani, N. T., Vengadaesvaran, B., Kariem Arof, A. Eds.; Elsevier, 2021; pp 139-178.

(89) Bolshakov, A. P.; Ralchenko, V. G.; Yurov, V. Y.; Popovich, A. F.; Antonova, I. A.; Khomich, A. A.; Ashkinazi, E. E.; Ryzhkov, S. G.; Vlasov, A. V.; Khomich, A. V. High-rate growth of single crystal diamond in microwave plasma in CH4/H2 and CH4/H2/Ar gas mixtures in presence of intensive soot formation. *Diamond and Related Materials* 2016, *62*, 49-57. DOI: https://doi.org/10.1016/j.diamond.2015.12.001.

(90) Tang, L.; Zhou, X.; Yue, R.; Wang, Y. N-type lithium-nitrogen codoping in diamond from first principles. In *2017 International Conference on Electron Devices and Solid-State Circuits (EDSSC)*, 18-20 Oct. 2017, 2017; pp 1-2. DOI: 10.1109/EDSSC.2017.8126459.

(91) Miyazaki, T.; Uda, T. Possible shallowing of nitrogen donors in diamond. *MRS Online Proceedings Library* 2011, *719* (1), 22. DOI: 10.1557/PROC-719-F2.2.

(92) Nakano, Y.; Zhang, X.; Kobayashi, K.; Matsumoto, T.; Inokuma, T.; Yamasaki, S.; Nebel, C. E.; Tokuda, N. Impact of nitrogen doping on homoepitaxial diamond (111) growth. *Diamond and Related Materials* 2022, *125*, 108997. DOI: https://doi.org/10.1016/j.diamond.2022.108997.

(93) Chatei, H.; Bougdira, J.; Rémy, M.; Alnot, P.; Bruch, C.; Krüger, J. K. Effect of nitrogen concentration on plasma reactivity and diamond growth in a H2・CH4・N2 microwave discharge.

Diamond and Related Materials 1997, *6* (1), 107-119. DOI: https://doi.org/10.1016/S0925-9635(96)00588-2.

(94) Zhou, D.; Tang, L.; Zhang, J.; Yue, R.; Wang, Y. n-type B-N Co-doping and N Doping in Diamond from First Principles. In *Computational Science – ICCS 2022*, Cham, 2022//, 2022; Groen, D., de Mulatier, C., Paszynski, M., Krzhizhanovskaya, V. V., Dongarra, J. J., Sloot, P. M. A., Eds.; Springer International Publishing: pp 530-540.

(95) Kosowska, M.; Pawłowska, S.; Sankaran, K. J.; Majchrowicz, D.; Haenen, K.; Dholakia, K.; Szczerska, M. Incorporation of nitrogen in diamond films – A new way of tuning parameters for optical passive elements. *Diamond and Related Materials* 2021, *111*, 108221. DOI: https://doi.org/10.1016/j.diamond.2020.108221.

(96) Zaitsev, A. M.; Kazuchits, N. M.; Kazuchits, V. N.; Moe, K. S.; Rusetsky, M. S.; Korolik, O. V.; Kitajima, K.; Butler, J. E.; Wang, W. Nitrogen-doped CVD diamond: Nitrogen concentration, color and internal stress. *Diamond and Related Materials* 2020, *105*, 107794. DOI: https://doi.org/10.1016/j.diamond.2020.107794.

(97) Croot, A.; Othman, M. Z.; Conejeros, S.; Fox, N. A.; Allan, N. L. A theoretical study of substitutional boron–nitrogen clusters in diamond. *Journal of Physics: Condensed Matter* 2018, *30* (42), 425501. DOI: 10.1088/1361-648X/aade16.

(98) Liu, D. Y.; Hao, L. C.; Teng, Y.; Qin, F.; Shen, Y.; Tang, K.; Ye, J. D.; Zhu, S. M.; Zhang, R.; Zheng, Y. D.; et al. Nitrogen modulation of boron doping behavior for accessible n-type diamond. *APL Materials* 2021, *9* (8). DOI: 10.1063/5.0049151 (acccessed 4/10/2024).

(99) Koeck, F. A. M.; Nemanich, R. J. Advances in Thermionic Energy Conversion through Single-Crystal n-Type Diamond. *Frontiers in Mechanical Engineering* 2017, *3*, Original Research. DOI: 10.3389/fmech.2017.00019.

(100) Gao, H.-X.; Li, J.-B.; Xia, J.-B. Origins of ferromagnetism in transition metal doped diamond. *Physica B: Condensed Matter* 2012, *407* (12), 2347-2350. DOI: https://doi.org/10.1016/j.physb.2012.03.035.

(101) Chevallier, J. Chapter 1 Hydrogen diffusion and acceptor passivation in diamond. In *Semiconductors and Semimetals*, Nebel, C. E., Ristein, J. Eds.; Vol. 77; Elsevier, 2004; pp 1-35.

(102) Segev, D.; Wei, S.-H. Design of Shallow Donor Levels in Diamond by Isovalent-Donor Coupling. *Physical Review Letters* 2003, *91* (12), 126406. DOI: 10.1103/PhysRevLett.91.126406.

(103) Zulkharnay, R.; Zulpukarova, G.; May, P. W. Oxygen-terminated diamond: insights into the correlation between surface oxygen configurations and work function values. *Applied Surface Science* 2024, *658*, 159776. DOI: https://doi.org/10.1016/j.apsusc.2024.159776.

(104) Yao, Y.; Sang, D.; Duan, S.; Wang, Q.; Liu, C. Review on the Properties of Boron-Doped Diamond and One-Dimensional-Metal-Oxide Based P-N Heterojunction. *Molecules* 2021, *26* (1), 71.